**Chapter D**

# Comparison of Kinetic-Model Predictions of Deep Gas Generation

*By* Allison A. Henry *and* Michael D. Lewan

*Prepared in cooperation with the U.S. Department of Energy–National Energy Technology Laboratory, the Gas Technology Institute, and Advanced Resources International*

U.S. Department of the Interior
U.S. Geological Survey

# Contents



# Figures

## Tables

# Comparison of Kinetic-Model Predictions of Deep Gas Generation

*By* Allison A. Henry[1] *and* Michael D. Lewan[2]

## Introduction

The origin of and processes resulting in natural gas generation remain a controversial issue in petroleum geochemistry (Price, 1997). Various investigations have used different pyrolysis methods and organic sources to develop models to predict timing and quantities of natural gas generation in sedimentary basins (table 1). The results and implications of these different models on predicting natural gas generation have not previously been compared in the literature. The objective of this study is to compare six different published gas-generation kinetic models (table 1) with respect to their predictions of timing and quantities of deep gas generation. As discussed by Dyman and others (1997), the potential for deep gas at depths greater than 15,000 feet/4,572 m remains an uncertain domestic exploration frontier. Two geologic settings for the occurrence of deep gas emerge from this definition. The first geologic setting envisages gas being initially generated and accumulating in traps at shallow depths (<15,000 feet/4,572 m). As sedimentation and basin subsidence continue with geologic time, these shallow traps remain coherent and are eventually buried to depths greater than 15,000 feet/4,572 m. Deep gas accumulations resulting from this setting are dependent on the competence of trap closures and seals with burial to depths greater than 15,000 feet/4,572 m. The second geologic setting envisages gas generation and accumulation in traps at deeper depths (>15,000 feet/4,572 m). Deep-gas accumulations resulting from this setting are dependent on a source of gas at burial depths greater than 15,000 feet/4,572 m. It is this dependence on sources of deep gas generation that this study examines.

Various kinetic models for the generation of natural gas in sedimentary basins have been published over the last several years. These gas-generation kinetic models are primarily based on different types of laboratory pyrolysis methods, which include open-system anhydrous pyrolysis (for example, Rock-Eval; Behar and others, 1997), closed-system anhydrous pyrolysis (for example, microscale sealed (MSSV) pyrolysis; Horsfield and others, 1992), and closed-system hydrous pyrolysis (flexible gold-bag autoclaves; Knauss and others, 1997). In addition to employing different pyrolysis methods, different starting materials are considered as the source of natural gas. Some kinetic models consider crude oil in deeply buried reservoirs (Tsuzuki and others, 1997), and others consider unexpelled oil retained in mature source rocks (Pepper and Corvi, 1995).

These kinetic models are examined in two hypothetical basin scenarios that represent end-member heating rates of 1° and 10°C/m.y. *This study makes no attempt to judge the validity of the six kinetic models used but only intends to present and compare their results and the implications they have on deep gas generation.* Kinetic models for the thermal stability of crude oil that are based on model hydrocarbons were not included in this study. Although studies of such models provide useful information on the influence of pressure, oil matrices, and cracking mechanisms (Domine, 1991; Behar and Vandenbroucke, 1996; Burnham and others, 1997), either they are based on the loss of the model compound rather than generated gas, or the generated gases have peculiar gas compositions significantly different from natural gases.

## Acknowledgments

This study was funded in part by the U.S. Department of Energy (National Energy Technology Laboratory, Morgantown, W.Va., contract No. DE-AT26-98FT40032), Gas Research Institute (Chicago, Ill.) as a Cooperative Research and Development Agreement with Advanced Resources International (Arlington, Va.), and the U.S. Geological Survey, Denver, Colo. The authors also appreciate the helpful reviews of this report made by John Curtis (Colorado School of Mines), Thaddeus Dyman (USGS), and Katharine Varnes (USGS).

## Methods

### Basin Scenarios

Gretener and Curtis (1982) have estimated common heating rates for sedimentary basins to be between 1° and 10°C/m.y. In keeping with these limits, the kinetic models used in this study are compared in two end-member basin scenarios. One basin scenario uses a thermal gradient of 30°C/km and burial rate of 33.3 m/m.y., which results in a heating rate of 1°C/m.y. The other scenario uses a thermal gradient of 45°C/km and burial rate of 222.2 m/m.y., which results in a heating rate of 10°C/m.y. The heating rates were assumed to be linear in both basin scenarios.

[1]Current Address: The Scripps Research Institute, 10550 North Torrey Pines Road, La Jolla, CA 92037. (<ahenry@scripps.edu>)

[2]<mlewan@usgs.gov>

**Table 1.** Summary of six gas-generation kinetic models considered in this study.

| Model name | Ref* | Starting material | Kinetic approach | Kinetic parameters |
|---|---|---|---|---|
| Open pyrolysis | 1 | Kerogen (Type-I, -II, -IIS, -III) | Optimization of non-isothermal experiments at different heating rates. | Discrete distribution of activation energies with single frequency factor. |
| Composite pyrolysis | 2 | Kerogen (Type-I, -II, -IIS, -III) | Optimization of open and anhydrous pyrolysis and natural data. | Gaussian distribution of activation energies with single frequency factor. |
| Hydrous pyrolysis | 3 | Kerogen (Type-II) | Optimization of isothermal pyrolysis experiments. | Gaussian distribution of activation energies with single frequency factor. |
| | 4 | Crude oil (light and heavy saturates) | Optimization of isothermal pyrolysis experiments. | Single activation energies and frequency factors for light and heavy saturates. |
| Anhydrous pyrolysis | 5 | Crude oil (36°API gravity) | Optimization of non-isothermal experiments at different heating rates. | Discrete distribution of activation energies with single frequency factor. |
| | 6 | Immature source rock (organofacies A, B, C, D/E, F) | Optimization of isothermal pyrolysis experiments at one temperature. | Gaussian distribution of activation energies with single frequency factor. |

* References: 1, Behar and others (1997); 2, Pepper and Corvi (1995); 3, Knauss and others (1997); 4, Tsuzuki and others (1997); 5, Horsfield and others (1992); 6, Pepper and Dodd (1995).

## Kinetic Models

Attributes of the six kinetic models considered in this study are given in table 1. Three of the models consider gas generation from kerogen (Behar and others, 1997; Pepper and Corvi, 1995; and Knauss and others, 1997). Behar and others (1997) used kerogen samples including a Type-I kerogen from the Eocene Green River Formation, Type-II kerogen from a Toarcian shale of the Paris basin, Type-IIS kerogen from the Miocene Monterey Formation, and two Type-III kerogens from a Miocene coal in the Mahakam delta and a Dogger coal from the North Sea. Pepper and Corvi (1995) organized their kerogen samples into organofacies A, B, C, D/E, and F. According to their definitions of organofacies, organofacies A kerogen is similar to Type-IIS kerogen, organofacies B kerogen is similar to Type-II kerogen, organofacies C kerogen is similar to Type-I kerogen, organofacies D/E is similar to Type-III kerogen, and organofacies F is similar to Type-III/IV kerogens. Knauss and others (1997) used New Albany Shale (Devonian-Mississippian), which contains Type-II kerogen.

The other three models consider gas generation from the cracking of oil (Horsfield and others, 1992; Pepper and Dodd, 1995; and Tsuzuki and others, 1997). Horsfield and others (1992) used a medium-gravity crude oil from a Middle Jurassic reservoir in the Central Graben of the Norwegian North Sea (NOCS 33/9-14). Pepper and Dodd (1995) focused on the in-source cracking of oil as opposed to the cracking of reservoir oils; the authors used 16 samples of source rocks classified as members of their five organofacies. Tsuzuki and others (1997) used a Sarukawa crude oil with an API gravity of 33.6°.

## Model/Pyrolysis Terminology

The four types of models in this study are based on different pyrolysis methods. The **open-pyrolysis** model uses Rock-Eval pyrolysis to determine kinetic parameters (Behar and others, 1997). The **composite-pyrolysis** model refers to Pepper and Corvi's (1995) mixed data set from many different references, natural data sets, and open- and closed-system pyrolysis methods. The **anhydrous-pyrolysis** model refers to closed-system pyrolysis of kerogen or oil without liquid water and is used by Pepper and Dodd (1995) and Horsfield and others (1992). The **hydrous-pyrolysis** model refers to pyrolysis of kerogen or oil in the presence of liquid water and is used by Knauss and others (1997) and Tsuzuki and others (1997).

## Extent of Reaction with Single Activation Energy and Frequency Factor

As demonstrated by Wood (1988), the extent of a reaction (that is, $k$=rate constant) that follows the Arrhenius equation,

$$k = A\exp\left(-\frac{E}{RT}\right)$$

can be reasonably estimated over a linear heating rate by the approximate analytical integral solution derived by Gorbachev (1975):

$$\begin{aligned}\mathrm{TTI_{ARR}} = &\left\{(A(t_{n+1}-t_n))/(T_{n+1}-T_n)\right\}* \\ &\left\{[(RT^2{}_{n+1}/(E+2RT_{n+1}))*\exp(-E/RT_{n+1})]\right. \\ &\left.-[(RT^2{}_n/(E+2RT_n))*\exp(-E/RT_n)]\right\}\end{aligned} \quad (1)$$

where $\mathrm{TTI_{ARR}}$ is the extent of reaction function or time-temperature index, $A$ is the frequency factor in m.y.$^{-1}$, $E$ is the activation energy in cal/mol, $R$ is the ideal gas constant in cal/mol-K, $t_n$ is the beginning of the time interval in m.y., $t_{n+1}$ is the end of the time interval in m.y., $T_n$ is the temperature in K at the start of the time interval, and $T_{n+1}$ is the temperature in K at the end of the time interval. $\mathrm{TTI_{ARR}}$ can be equated to the integrated first order rate equation,

$$\ln(1/[1-X]) = kt, \quad (2)$$

by

$$\mathrm{TTI_{ARR}} = \ln(1/[1-X]) \quad (3)$$

where $X$ represents the extent of reaction as a decimal fraction, which is referred to as fraction of reaction. $\mathrm{TTI_{ARR}}$ values can be calculated for various intervals in the burial history of a potential source rock using equation 1. The $\mathrm{TTI_{ARR}}$ calculated for each burial interval is additive, and the sum values can be converted to fraction of reaction by solving equation 3 for $X$:

$$X = 1 - (1/\exp[\mathrm{TTI_{ARR}}]). \quad (4)$$

Tsuzuki and others (1997) derived single $E$ and $A$ values for the generation of $C_1$–$C_5$ hydrocarbon gas from the cracking of light ($C_6$–$C_{14}$ saturates) and heavy ($C_{15+}$ saturates) components of crude oil. The activation energy and frequency factor for the cracking of the light component are respectively 86 kcal/mol and $6.4868\times10^{35}$ m.y.$^{-1}$ The activation energy and frequency factor for the cracking of the heavy component are respectively 76 kcal/mol, $3.4187\times10^{33}$ m.y.$^{-1}$ These kinetic parameters and the two end-member heating rates were used in equation 1 to determine the extent of gas generation from the cracking of oil in the two basin scenarios.

## Extent of Reaction using Multiple Activation Energies or Frequency Factors

In order to reflect a first-order reaction with more than one frequency factor or activation energy, $X$ of equation 4 must also represent the fractional extent of reaction for each activation energy and frequency factor. Multiple activation energies or frequency factors are derived by curve-fitting methods that assume first-order parallel reactions. The multiple kinetic parameters are described as discrete or Gaussian distributions, wherein each of the multiple parameters is assigned a fractional part of the overall reaction (Ungerer and others, 1986; Braum and Burnham, 1987).

The discrete distribution is used by Behar and others (1997) and Horsfield and others (1992). Both groups optimized their experimental kinetic data in such a way as to give a variety of activation energies with associated fractions of reaction and a single frequency factor. Behar and others (1997) presented discrete activation-energy distributions for the generation of methane ($C_1$) and $C_2$–$C_5$ hydrocarbon gas from five kerogens (table 2). Horsfield and others (1992) also used a discrete activation-energy distribution between 50 and 73 kcal/mol with a frequency factor of $3.47\times10^{29}$ m.y.$^{-1}$ for oil cracking to $C_1$–$C_4$ hydrocarbon gas (table 3). Equation 1 is used for each discrete activation energy for the fractional part of the reaction it is assigned and then summed with results from the other discrete activation energies to give a cumulative generation curve for the extent of reaction.

The Gaussian distribution of activation energies is employed by Pepper and Dodd (1995), Pepper and Corvi (1995), and Knauss and others (1997). The distribution is presented by a mean activation energy, $E_{mean}$, and a standard deviation, $\sigma_E$, as shown in table 4. A Gaussian distribution is expressed by the equation

$$Y = \frac{1}{\sigma\sqrt{2\Pi}} e^{-\frac{1}{2}(X-\mu)^2/\sigma^2} \quad (5)$$

where $\sigma$ is the standard deviation at the 68 percent confidence level ($\sigma_E$), $\mu$ is the mean activation energy ($E_{mean}$), and $Y$ is the height of the curve above a given $X$ (discrete activation energy). The function reaches a maximum value of

$$\frac{1}{\sigma\sqrt{2\Pi}}$$

when $X=\mu$. Using equation 5 and the parameters given by the cited authors, the Gaussian distribution was divided into discrete 1.0-kcal/mol activation energies. As the area under the normal curve is one and each rectangle of discrete activation energy is one unit wide, the area of the rectangle becomes the fractional part of the reaction for a given discrete activation energy. When summed, the values at each discrete energy will equal 1. Equation 1 is used for each discrete activation energy to determine the fractional part of the reaction it is assigned and then summed with results from the other discrete activation energies to give a cumulative generation curve for the extent of reaction. Pepper and Corvi (1995) and Knauss and others (1997) used a different single frequency factor with each distribution, but Pepper and Dodd (1995) used the same single frequency factor for all of their activation energy distributions (table 4).

## Amount of Gas Generated

All the kinetic models considered in this study employ first-order reaction rates, which give the extent of reaction, $X$, as a decimal fraction of the completed reaction at unity (that is, $X$ equals amount of gas generated at a particular thermal stress divided by the maximum amount of gas that can be generated from a particular source material). The obvious question that remains is, how much gas per mass of starting material does unity equal? Behar and others (1997) explicitly stated the maximum amounts ($X$=1) of $C_1$ and $C_2$–$C_5$ generated from kerogen, as given in table 5. These values were combined to give maximum yields for $C_1$–$C_5$ in milligrams per gram of total organic carbon (mg/g C). Pepper and Corvi (1995) gave maximum $C_1$–$C_5$ gas generation for each of their five organofacies: A=105 mg/g C; B=101 mg/g C; C=78 mg/g C; D/E=77 mg/g C; and F=70 mg/g C.

The maximum gas concentrations reported as mmolal for the hydrous-pyrolysis experiments by Knauss and others (1997) are converted to mg/g C by the equation

$$\text{Gas(mg/gC)} = \frac{MW\times G_{mmolal}\times\frac{w}{s}}{1000\times\text{TOC}} \quad (6)$$

where $MW$ is the formula weight of the gas component (that is, $C_1$=16.04 g/mol, $C_2$=30.07 g/mol, $C_3$=44.10 g/mol, and $C_4$=58.12 g/mol), $G_{mmolal}$ is the maximum gas yield in mmolal (Knauss and others, 1997; table 2, p. 482–483), $w/s$ is the water:shale ratio at time zero for the experiments (4.06 g/g), and TOC is the total organic carbon of the rock expressed as a fraction (0.114). Equation 6 gives maximum gas yields of 26.5 mg/g C for methane ($C_1$), 24.9 mg/g C for ethane ($C_2$), 22.0 mg/g C for propane ($C_3$) and 19.4 mg/g C for butane ($C_4$). The total of these values (92.8 mg/g C) gives the maximum $C_1$–$C_4$ gas generated from the New Albany Shale (table 5).

According to Pepper and Dodd (1995), the maximum amount of $C_1$–$C_5$ gas generated from the cracking of oil in a source rock is equivalent to the amount of oil remaining in the kerogen after expulsion. Therefore, the maximum amount of gas for all 16 kerogen samples is 100 mg/g C, which they considered the threshold for oil retained by sorption in the kerogen (A.S. Pepper, pers. commun., 1998).

Horsfield and others (1992) experimentally determined that the maximum amount of $C_1$–$C_4$ gas generated from the cracking of reservoired oil by closed-system anhydrous pyrolysis is 460 mg/g oil. Tsuzuki and others (1997) considered gas generation from the cracking of reservoired Sarukawa oil by closed-system hydrous pyrolysis. The generation of $C_1$–$C_5$ gas is described by two reactions. One reaction ($k$11) involves the conversion of $C_{15+}$ heavy saturates ($C_{15+}$Sat) to $C_{15+}$ heavy condensed aromatics ($C_{15+}$Aro), $C_1$–$C_5$ gas ($C_1$–$C_5$), and $C_6$–$C_{14}$ light saturates ($C_6$–$C_{14}$Sat):

$$C_{15+}\text{ Sat} \xrightarrow{k11} 0.36(C_{15+}\text{Aro})+0.27(C_1\text{–}C_5)+0.37(C_6\text{–}C_{14}\text{Sat}) \quad (7)$$

The other reaction ($k$2) involves the conversion of the generated $C_6$–$C_{14}$ light saturates ($C_6$–$C_{14}$Sat) generated in reaction 7 to $C_1$–$C_5$ gas ($C_1$–$C_5$) and insoluble coke (C  ):

$$C_6\text{–}C_{14}\text{ Sat} \xrightarrow{k2} 0.60(C_1\text{–}C_5)+0.40(C\text{--}). \quad (8)$$

Jamil and others (1991) reported that $C_{15+}$ heavy saturates ($C_{15+}$Sat) compose 64.9 wt. percent of Sarukawa oils. Therefore, 1 g of oil will initially generate 175 mg of $C_1$–$C_5$ gas through the cracking of $C_{15+}$ heavy saturates ($C_{15+}$Sat; equation 7) and an additional 144 mg of $C_1$–$C_5$ gas through the cracking of $C_6$–$C_{14}$ light saturates ($C_6$–$C_{14}$Sat; equation 8). These two values are combined to give 319 mg/g oil as the maximum amount of gas generated from the cracking of oil.

**Table 2.** Fractional gas yields assigned to discrete activation energies and single-frequency factors used by Behar and others (1997) to model gas generation from kerogen.

| | Fractional Part of Total Gas Yield | | | | | | | | | |
|---|---|---|---|---|---|---|---|---|---|---|
| | Type-I kerogen | | Type-II kerogen | | Type-IIS kerogen | | Type-III' kerogen | | Type-III kerogen | |
| | $C_1$ | $C_2$–$C_5$ | $C_1$ | $C_2$–$C_5$ | $C_1$ | $C_2$–$C_5$ | $C_1$ | $C_2$–$C_5$ | $C_1$ | $C_2$–$C_5$ |
| Activation energy (kcal/mol) | Fractional gas yield | Fractional gas yield | Fractional gas yield | Fractional gas yield | Fractional gas yield | Fractional gas yield | Fractional gas yield | Fractional gas yield | Fractional gas yield | Fractional gas yield |
| 74.0 | 0.00 | 0.00 | 0.00 | 0.00 | 0.00 | 0.00 | 0.00 | 0.00 | 0.032 | 0.00 |
| 72.0 | 0.00 | 0.00 | 0.00 | 0.00 | 0.00 | 0.00 | 0.02 | 0.00 | 0.126 | 0.01 |
| 70.0 | 0.00 | 0.00 | 0.00 | 0.00 | 0.00 | 0.00 | 0.13 | 0.00 | 0.133 | 0.06 |
| 68.0 | 0.00 | 0.00 | 0.00 | 0.002 | 0.00 | 0.00 | 0.16 | 0.02 | 0.136 | 0.05 |
| 66.0 | 0.02 | 0.00 | 0.02 | 0.006 | 0.004 | 0.00 | 0.16 | 0.04 | 0.159 | 0.10 |
| 64.0 | 0.08 | 0.00 | 0.07 | 0.014 | 0.019 | 0.00 | 0.16 | 0.07 | 0.155 | 0.18 |
| 62.0 | 0.08 | 0.00 | 0.11 | 0.024 | 0.034 | 0.00 | 0.14 | 0.17 | 0.129 | 0.25 |
| 60.0 | 0.10 | 0.00 | 0.13 | 0.040 | 0.174 | 0.01 | 0.11 | 0.28 | 0.094 | 0.24 |
| 58.0 | 0.12 | 0.00 | 0.19 | 0.092 | 0.159 | 0.03 | 0.07 | 0.22 | 0.032 | 0.11 |
| 56.0 | 0.19 | 0.00 | 0.15 | 0.225 | 0.186 | 0.05 | 0.03 | 0.13 | 0.003 | 0.02 |
| 54.0 | 0.38 | 0.95 | 0.15 | 0.247 | 0.144 | 0.19 | 0.01 | 0.05 | 0.00 | 0.00 |
| 52.0 | 0.02 | 0.05 | 0.11 | 0.241 | 0.080 | 0.27 | 0.00 | 0.02 | 0.00 | 0.00 |
| 50.0 | 0.00 | 0.00 | 0.05 | 0.092 | 0.080 | 0.16 | 0.00 | 0.01 | 0.00 | 0.00 |
| 48.0 | 0.00 | 0.00 | 0.02 | 0.016 | 0.068 | 0.21 | 0.00 | 0.00 | 0.00 | 0.00 |
| 46.0 | 0.00 | 0.00 | 0.00 | 0.002 | 0.042 | 0.06 | 0.00 | 0.00 | 0.00 | 0.00 |
| 44.0 | 0.00 | 0.00 | 0.00 | 0.00 | 0.011 | 0.01 | 0.00 | 0.00 | 0.00 | 0.00 |
| Frequency factor (1/m.y.) | 2.33E+27 | 2.33E+27 | 5.05E+27 | 5.05E+27 | 7.88E+26 | 7.88E+26 | 9.46E+28 | 9.46E+28 | 9.78E+28 | 9.78E+28 |
| Total gas yields | 16.4 mg/g C | 72.1 mg/g C | 18.8 mg/g C | 50.2 mg/g C | 26.4 mg/g C | 43.9 mg/g C | 30.6 mg/g C | 23.6 mg/g C | 30.9 mg/g C | 26.2 mg/g C |

**Table 3.** Fractional $C_1$–$C_4$ gas yields assigned to discrete activation energies by Horsfield and others (1992) to model gas generation from the cracking of oil.

| Activation energy (kcal/mol) | Fractional gas yields |
|---|---|
| 73 | 0.0174 |
| 72 | 0.0087 |
| 70 | 0.0587 |
| 69 | 0.1109 |
| 68 | 0.1478 |
| 67 | 0.2870 |
| 66 | 0.3435 |
| 63 | 0.0043 |
| 58 | 0.0065 |
| 55 | 0.0022 |
| 54 | 0.0022 |
| 53 | 0.0043 |
| 51 | 0.0022 |
| 50 | 0.0022 |
| Frequency factor (1/m.y.) | 3.47E+29 |
| Total gas yield | 460 mg/g oil |

# Results

## Kerogen to Gas

Figure 1 shows the gas-generation curves for Type-I kerogens in basins with 1° and 10°C/m.y. heating rates as predicted by the open- and composite-pyrolysis models. At the top of the deep gas depth (15,000 feet/4,572 m), 91 and 64 percent of gas generation from Type-I kerogen are completed at 1°C/m.y. according to the open- and composite-pyrolysis models, respectively. Therefore, 7.9 and 27.9 mg/g C of deep gas are generated according to the open- and composite-pyrolysis models, respectively (fig. 1*A* and table 6). Both models predict that the deep gas generation is finished (that is, $X$=0.99) at depths of 22,310 and 18,373 feet (6,800 and 5,600 m) (table 6). At the top of the deep gas depth (15,000 feet/4,572 m), the open- and composite-pyrolysis models respectively predict that 99 and 100 percent of gas generation from Type-I kerogen are completed at 10°C/m.y. According to these models, essentially no deep gas is generated from Type-I kerogen at this heating rate.

Figure 2 shows the gas-generation curves for Type-II kerogens in basins with 1° and 10°C/m.y. heating rates as predicted by the open- and composite-pyrolysis models. At the top of the deep gas depth (15,000 feet/4,572 m), 75, 67, and 35 percent of gas generation from Type-II kerogen are completed at 1°C/m.y. according to the hydrous-, open-, and composite-pyrolysis models, respectively. These percentages indicate that 23.0, 22.9, and 65.0 mg/g C of deep gas are generated according to the hydrous-, open-, and composite-pyrolysis models, respectively (fig. 2*A* and table 6). Deep gas generation is finished (that is, $X$=0.99) according to these three models at depths of 19,029, 22,310, and 23,622 feet (5,800, 6,800, and 7,200 m) (table 6). At the top of the deep gas depth (15,000 feet/4,572 m), the open- and composite-pyrolysis models predict 92, 97, 95, and 100 percent of gas generation from Type-II kerogen completed at 10°C/m.y., respectively. Therefore, according to these models, essentially no significant amounts of deep gas are generated from Type-II kerogen at this heating rate.

Figure 3 shows the gas-generation curves for Type-IIS kerogens in basins with 1° and 10°C/m.y. heating rates as predicted by the open- and composite-pyrolysis models. At the top of the deep gas depth (15,000 feet/4,572 m), 74 and 93 percent of gas generation from Type-IIS kerogen are completed at 1°C/m.y. according to the open- and composite-pyrolysis models, respectively. Therefore, 17.9 and 7.0 mg/g C of deep gas are generated according to the open- and composite-pyrolysis models, respectively (fig. 3*A* and table 6). These models predict that the deep gas generation is finished (that is, $X$=0.99) at depths of 20,997 and 16,404 feet (6,400 and 5,000 m) (table 6). At the top of the deep gas depth (15,000 feet/4,572 m), the open- and composite-pyrolysis models predict 99 and 100 percent of gas generation from Type-IIS kerogen completed at 10°C/m.y., respectively. Therefore, essentially no deep gas is generated from Type-IIS kerogen at this heating rate.

Figure 4 shows the gas-generation curves for Type-III kerogens in basins with 1° and 10 °C/m.y. heating rates as predicted by the open- and composite-pyrolysis models. At the top of the deep gas depth (15,000 feet/4,572 m), 26 and 3 percent of gas generation from Type-III kerogen are completed at 1°C/m.y. according to the open- and composite-pyrolysis models, respectively. Therefore, 39.7 and 73.8 mg/g C of deep gas are generated according to the open- and composite-pyrolysis models, respectively (fig. 4*A* and table 6). These models predict that the deep gas generation is finished (that is, $X$=0.99) at depths of 20,997 and 22,966 feet (6,400 and 7,000 m) (table 6). At the top of the deep gas depth (15,000 feet/4,572 m), the open- and composite-pyrolysis models predict 85 and 92 percent of gas generation from Type-III kerogen completed at 10°C/m.y., respectively. According to these models, 7.9 and 6.0 mg/g C of deep gas are generated from Type-III kerogen at this heating rate.

Figure 5 shows the gas-generation curves for more paraffinic Type-III kerogens (Type-III′) in basins with 1° and 10 °C/m.y. heating rates as predicted by the open- and composite-pyrolysis models. At the top of the deep gas depth (15,000 feet/4,572 m), 11 and 3 percent of gas generation from Type-III′ kerogen are completed at 1°C/m.y. according to the open- and composite-pyrolysis models, respectively. Therefore, 50.6 and 67.7 mg/g C of deep gas are generated according to the open- and composite-pyrolysis models, respectively (fig. 5*A* and table 6). These models predict that the deep gas generation is finished (that is, $X$=0.99) at depths of 25,591 and 22,966 feet (7,800 and 7,000 m) (table 6). At the top of the deep gas depth (15,000 feet/4,572 m), the open- and composite-pyrolysis models predict 74 and 91 percent of gas generation from Type-III kerogen completed at 10°C/m.y., respectively. According to these models, 14.9 and 6.0 mg/g C of deep gas are generated from Type-III′ kerogen at this heating rate.

**Table 4a.** Gaussian distributions and their calculated discrete distributions of activation energies with fractional $C_1$–$C_5$ gas yield from kerogens as predicted by the composite-pyrolysis model (Pepper and Corvi, 1995).

| Organofacies A Type-IIS | | Organofacies B Type-II | | Organofacies C Type-I | | Organofacies F/DE Type-III/III' | |
|---|---|---|---|---|---|---|---|
| Gaussian distribution of activation energies (kcal/mol) | | Gaussian distribution of activation energies (kcal/mol) | | Gaussian distribution of activation energies (kcal/mol) | | Gaussian distribution of activation energies (kcal/mol) | |
| mean | 49.4 | mean | 66.6 | mean | 59.8 | mean | 65.7 |
| std.dev. | 2.6 | std.dev. | 4.4 | std.dev. | 2.4 | std.dev. | 2.4 |
| Discrete distribution | | Discrete distribution | | Discrete distribution | | Discrete distribution | |
| Activation energies (kcal/mol) | Fractional gas yield | Activation energies (kcal/mol) | Fractional gas yield | Activation energies (kcal/mol) | Fractional gas yield | Activation energies (kcal/mol) | Fractional gas yield |
| 56.4 | 0.0037 | 77.6 | 0.0040 | 65.8 | 0.0079 | 71.7 | 0.0070 |
| 55.4 | 0.0100 | 76.6 | 0.0069 | 64.8 | 0.0201 | 70.7 | 0.0185 |
| 54.4 | 0.0231 | 75.6 | 0.0112 | 63.8 | 0.0432 | 69.7 | 0.0412 |
| 53.4 | 0.0460 | 74.6 | 0.0174 | 62.8 | 0.0782 | 68.7 | 0.0766 |
| 52.4 | 0.0785 | 73.6 | 0.0257 | 61.8 | 0.1191 | 67.7 | 0.1191 |
| 51.4 | 0.1150 | 72.6 | 0.0359 | 60.8 | 0.1529 | 66.7 | 0.1549 |
| 50.4 | 0.1446 | 71.6 | 0.0477 | 59.8 | 0.1652 | 65.7 | 0.1686 |
| 49.4 | 0.1560 | 70.6 | 0.0601 | 58.8 | 0.1504 | 64.7 | 0.1535 |
| 48.4 | 0.1445 | 69.6 | 0.0720 | 57.8 | 0.1154 | 63.7 | 0.1168 |
| 47.4 | 0.1148 | 68.6 | 0.0819 | 56.8 | 0.0745 | 62.7 | 0.0744 |
| 46.4 | 0.0783 | 67.6 | 0.0885 | 55.8 | 0.0405 | 61.7 | 0.0396 |
| 45.4 | 0.0458 | 66.6 | 0.0907 | 54.8 | 0.0186 | 60.7 | 0.0177 |
| 44.4 | 0.0230 | 65.6 | 0.0884 | 53.8 | 0.0072 | 59.7 | 0.0066 |
| 43.4 | 0.0099 | 64.6 | 0.0817 | 52.8 | 0.0000 | 58.7 | 0.0000 |
| 42.4 | 0.0037 | 63.6 | 0.0718 | 51.8 | 0.0000 | 57.7 | 0.0000 |
| 41.5 | 0.0000 | 62.6 | 0.0598 | 50.8 | 0.0000 | 56.7 | 0.0000 |
| 40.5 | 0.0000 | 61.6 | 0.0474 | 49.8 | 0.0000 | 55.7 | 0.0000 |
| 39.5 | 0.0000 | 60.6 | 0.0356 | 48.8 | 0.0000 | 54.7 | 0.0000 |
| 38.5 | 0.0000 | 59.6 | 0.0255 | 47.8 | 0.0000 | 53.7 | 0.0000 |
| 37.5 | 0.0000 | 58.6 | 0.0173 | 46.8 | 0.0000 | 52.7 | 0.0000 |
| 36.5 | 0.0000 | 57.6 | 0.0111 | 45.8 | 0.0000 | 51.7 | 0.0000 |
| 35.5 | 0.0000 | 56.6 | 0.0068 | 44.8 | 0.0000 | 50.7 | 0.0000 |
| 34.5 | 0.0000 | 55.6 | 0.0039 | 43.8 | 0.0000 | 49.7 | 0.0000 |
| Frequency factor (1/m.y.) | 1.24E+26 | | 6.84E+31 | | 7.22E+29 | | 6.09E+29 |

## Source-Rock Oil to Gas

The anhydrous-pyrolysis model by Pepper and Dodd (1995) considers the kinetics of gas generation exclusively from the cracking of unexpelled oil retained in a source rock after the main stages of oil generation and expulsion are completed. Figure 6 shows their model's predicted gas-generation curves for oil retained in 16 source rocks in basins with 1° and 10°C/m.y. heating rates. These gas-generation curves are similar for all 16 source rocks irrespective of kerogen type or rock mineralogy.

**Table 4b.** Gaussian distributions and their calculated discrete distributions of activation energies with fractional $C_1$–$C_5$ gas yields from oil retained in mature source rocks as predicted by the anhydrous-pyrolysis model (Pepper and Dodd, 1995). Frequency factor (1/m.y.) for all source rocks is $3.15 \times 10^{27}$.

[BL, Brown Limestone; SM, St. Medard; Ha, Haltenbanken; LC9, LC995; Ta, Tarakan; CO, COST; AWD, PAL, not given]

| Source rock | BL | SM | Source rock | AWD | Ha | Source rock | PAL | LC9 | Ta | CO |
|---|---|---|---|---|---|---|---|---|---|---|
| Gaussian distribution | | | Gaussian distribution | | | Gaussian distribution | | | | |
| Activation energies (kcal/mol) | | | Activation energies (kcal/mol) | | | Activation energies (kcal/mol) | | | | |
| Mean | 58.7 | 57.7 | Mean | 58.4 | 56.4 | Mean | 58.1 | 57.1 | 58.1 | 57.1 |
| Std. dev. | 1.7 | 2.9 | Std. dev. | 2.4 | 3.6 | Std. dev. | 2.2 | 3.6 | 2.6 | 2.4 |
| Discrete distribution | | | Discrete distribution | | | Discrete distribution | | | | |
| Activation energy (kcal/mol) | Fractional gas yield | | Activation energy (kcal/mol) | Fractional gas yield | | Activation energy (kcal/mol) | Fractional gas yield | | | |
| 65.7 | 0.0000 | 0.0030 | 68.4 | 0.0000 | 0.0000 | 68.1 | 0.0000 | 0.0000 | 0.0000 | 0.0000 |
| 64.7 | 0.0000 | 0.0073 | 67.4 | 0.0000 | 0.0000 | 67.1 | 0.0000 | 0.0022 | 0.0000 | 0.0000 |
| 63.7 | 0.0026 | 0.0161 | 66.4 | 0.0000 | 0.0000 | 66.1 | 0.0000 | 0.0046 | 0.0000 | 0.0000 |
| 62.7 | 0.0132 | 0.0313 | 65.4 | 0.0022 | 0.0048 | 65.1 | 0.0000 | 0.0089 | 0.0043 | 0.0000 |
| 61.7 | 0.0466 | 0.0537 | 64.4 | 0.0069 | 0.0093 | 64.1 | 0.0037 | 0.0161 | 0.0110 | 0.0024 |
| 60.7 | 0.1147 | 0.0818 | 63.4 | 0.0182 | 0.0166 | 63.1 | 0.0122 | 0.0268 | 0.0245 | 0.0073 |
| 59.7 | 0.1977 | 0.1102 | 62.4 | 0.0401 | 0.0275 | 62.1 | 0.0323 | 0.0413 | 0.0471 | 0.0191 |
| 58.7 | 0.2384 | 0.1316 | 61.4 | 0.0745 | 0.0422 | 61.1 | 0.0691 | 0.0588 | 0.0784 | 0.0418 |
| 57.7 | 0.2011 | 0.1391 | 60.4 | 0.1162 | 0.0598 | 60.1 | 0.1193 | 0.0775 | 0.1129 | 0.0768 |
| 56.7 | 0.1187 | 0.1302 | 59.4 | 0.1520 | 0.0785 | 59.1 | 0.1657 | 0.0945 | 0.1407 | 0.1185 |
| 55.7 | 0.0490 | 0.1079 | 58.4 | 0.1669 | 0.0953 | 58.1 | 0.1855 | 0.1066 | 0.1517 | 0.1535 |
| 54.7 | 0.0142 | 0.0792 | 57.4 | 0.1538 | 0.1071 | 57.1 | 0.1672 | 0.1113 | 0.1416 | 0.1669 |
| 53.7 | 0.0029 | 0.0515 | 56.4 | 0.1190 | 0.1113 | 56.1 | 0.1215 | 0.1074 | 0.1143 | 0.1523 |
| 52.7 | 0.0000 | 0.0296 | 55.4 | 0.0773 | 0.1070 | 55.1 | 0.0711 | 0.0960 | 0.0799 | 0.1167 |
| 51.7 | 0.0000 | 0.0151 | 54.4 | 0.0422 | 0.0952 | 54.1 | 0.0335 | 0.0793 | 0.0483 | 0.0750 |
| 50.7 | 0.0000 | 0.0068 | 53.4 | 0.0193 | 0.0783 | 53.1 | 0.0127 | 0.0606 | 0.0253 | 0.0405 |
| 49.7 | 0.0000 | 0.0027 | 52.4 | 0.0074 | 0.0596 | 52.1 | 0.0039 | 0.0429 | 0.0114 | 0.0184 |
| 48.7 | 0.0000 | 0.0000 | 51.4 | 0.0024 | 0.0420 | 51.1 | 0.0000 | 0.0281 | 0.0045 | 0.0070 |
| 47.7 | 0.0000 | 0.0000 | 50.4 | 0.0000 | 0.0274 | 50.1 | 0.0000 | 0.0170 | 0.0000 | 0.0022 |
| 46.7 | 0.0000 | 0.0000 | 49.4 | 0.0000 | 0.0165 | 49.1 | 0.0000 | 0.0095 | 0.0000 | 0.0000 |
| 45.7 | 0.0000 | 0.0000 | 48.4 | 0.0000 | 0.0092 | 48.1 | 0.0000 | 0.0049 | 0.0000 | 0.0000 |
| 44.7 | 0.0000 | 0.0000 | 47.4 | 0.0000 | 0.0047 | 47.1 | 0.0000 | 0.0024 | 0.0000 | 0.0000 |

**Table 4b—Continued.** Gaussian distributions and their calculated discrete distributions of activation energies with fractional $C_1$–$C_5$ gas yields from oil retained in mature source rocks as predicted by the anhydrous-pyrolysis model (Pepper and Dodd, 1995). Frequency factor (1/m.y.) for all source rocks is $3.15 \times 10^{27}$.

[LC1, LC1005; Tu, Tuna; GA, Garlin; P5, Pematang 52.7; KCF, not given; Maui, Maui; WE, Westfield; P4, Pematang 45.2]

| Source rock | LC1 | Tu | | GA | KCF | P5 | Maui | WE | | P4 |
|---|---|---|---|---|---|---|---|---|---|---|
| Gaussian distribution | | | Gaussian distribution | | | | | | Gaussian distribution | |
| Activation energies (kcal/mol) | | | Activation energies (kcal/mol) | | | | | | Activation energies (kcal/mol) | |
| Mean | 57.3 | 58.3 | Mean | 56.6 | 58.6 | 58.6 | 57.6 | 57.6 | Mean | 58.8 |
| Std. dev. | 2.9 | 2.4 | Std. dev. | 4.8 | 2.6 | 1.9 | 3.6 | 4.3 | Std. dev. | 1.2 |
| Discrete distribution | | | Discrete distribution | | | | | | Discrete distribution | |
| Activation energy (kcal/mol) | Fractional gas yield | | Activation energy (kcal/mol) | Fractional gas yield | | | | | Activation energy (kcal/mol) | Fractional gas yield |
| 68.3 | 0.0000 | 0.0000 | 68.6 | 0.0037 | 0.0000 | 0.0000 | 0.0000 | 0.0035 | 68.8 | 0.0000 |
| 67.3 | 0.0000 | 0.0000 | 67.6 | 0.0060 | 0.0000 | 0.0000 | 0.0023 | 0.0062 | 67.8 | 0.0000 |
| 66.3 | 0.0000 | 0.0000 | 66.6 | 0.0095 | 0.0000 | 0.0000 | 0.0048 | 0.0104 | 66.8 | 0.0000 |
| 65.3 | 0.0028 | 0.0023 | 65.6 | 0.0144 | 0.0042 | 0.0000 | 0.0092 | 0.0165 | 65.8 | 0.0000 |
| 64.3 | 0.0069 | 0.0073 | 64.6 | 0.0209 | 0.0108 | 0.0014 | 0.0165 | 0.0247 | 64.8 | 0.0000 |
| 63.3 | 0.0152 | 0.0190 | 63.6 | 0.0290 | 0.0241 | 0.0064 | 0.0274 | 0.0351 | 63.8 | 0.0000 |
| 62.3 | 0.0298 | 0.0416 | 62.6 | 0.0384 | 0.0465 | 0.0223 | 0.0421 | 0.0472 | 62.8 | 0.0012 |
| 61.3 | 0.0517 | 0.0766 | 61.6 | 0.0488 | 0.0776 | 0.0588 | 0.059 | 0.0602 | 61.8 | 0.0142 |
| 60.3 | 0.0795 | 0.1183 | 60.6 | 0.0593 | 0.1122 | 0.1179 | 0.0784 | 0.0727 | 60.8 | 0.0818 |
| 59.3 | 0.1082 | 0.1534 | 59.6 | 0.0689 | 0.1402 | 0.1798 | 0.0952 | 0.0832 | 59.8 | 0.2345 |
| 58.3 | 0.1303 | 0.1669 | 58.6 | 0.0768 | 0.1517 | 0.2086 | 0.107 | 0.0903 | 58.8 | 0.3338 |
| 57.3 | 0.1391 | 0.1525 | 57.6 | 0.0818 | 0.1420 | 0.1841 | 0.1113 | 0.0927 | 57.8 | 0.2360 |
| 56.3 | 0.1314 | 0.1169 | 56.6 | 0.0835 | 0.1150 | 0.1236 | 0.1070 | 0.0903 | 56.8 | 0.0828 |
| 55.3 | 0.1100 | 0.0752 | 55.6 | 0.0815 | 0.0806 | 0.0631 | 0.0952 | 0.0832 | 55.8 | 0.0144 |
| 54.3 | 0.0815 | 0.0406 | 54.6 | 0.0762 | 0.0489 | 0.0245 | 0.0784 | 0.0727 | 54.8 | 0.0012 |
| 53.3 | 0.0535 | 0.0184 | 53.6 | 0.0681 | 0.0257 | 0.0072 | 0.0597 | 0.0602 | 53.8 | 0.0000 |
| 52.3 | 0.0311 | 0.0070 | 52.6 | 0.0583 | 0.0117 | 0.0016 | 0.0421 | 0.0472 | 52.8 | 0.0000 |
| 51.3 | 0.0160 | 0.0022 | 51.6 | 0.0478 | 0.0046 | 0.0000 | 0.0274 | 0.0351 | 51.8 | 0.0000 |
| 50.3 | 0.0073 | 0.0000 | 50.6 | 0.0375 | 0.0000 | 0.0000 | 0.0165 | 0.0247 | 50.8 | 0.0000 |
| 49.3 | 0.0029 | 0.0000 | 49.6 | 0.0282 | 0.0000 | 0.0000 | 0.0092 | 0.0165 | 49.8 | 0.0000 |
| 48.3 | 0.0000 | 0.0000 | 48.6 | 0.0203 | 0.0000 | 0.0000 | 0.0048 | 0.0104 | 48.8 | 0.0000 |
| 47.3 | 0.0000 | 0.0000 | 47.6 | 0.0139 | 0.0000 | 0.0000 | 0.0023 | 0.0062 | 47.8 | 0.0000 |
| 46.3 | 0.0000 | 0.0000 | 46.6 | 0.0092 | 0.0000 | 0.0000 | 0.0000 | 0.0035 | 46.8 | 0.0000 |
| 45.3 | 0.0000 | 0.0000 | 45.6 | 0.0058 | 0.0000 | 0.0000 | 0.0000 | 0.0000 | 45.8 | 0.0000 |
| 44.3 | 0.0000 | 0.0000 | 44.6 | 0.0035 | 0.0000 | 0.0000 | 0.0000 | 0.0000 | 44.8 | 0.0000 |

**Table 4c.** Gaussian distributions and their calculated discrete distributions of activation energies with fractional methane ($C_1$), ethane ($C_2$), propane ($C_3$), and butane ($C_4$) yields from Type-II kerogen in the New Albany Shale (Devonian-Mississippian) as predicted by the hydrous-pyrolysis model (Knauss and others, 1997).

| Methane ($C_1$) | | Ethane ($C_2$) | | Propane ($C_3$) | | Butane ($C_4$) | |
|---|---|---|---|---|---|---|---|
| Gaussian distribution | | Gaussian distribution | | Gaussian distribution | | Gaussian distribution | |
| E (kcal/mol) | 45.2 | E (kcal/mol) | 56.2 | E (kcal/mol) | 52.9 | E (kcal/mol) | 55.0 |
| Std. dev.(%E) | 1.92 | Std. dev.(%E) | 5.0 | Std. dev.(%E) | 6.0 | Std. dev.(%E) | 5.0 |
| Discrete distribution | | Discrete distribution | | Discrete distribution | | Discrete distribution | |
| Activation energies (kcal/mol) | Fractional gas yield | Activation energies (kcal/mol) | Fractional gas yield | Activation energies (kcal/mol) | Fractional gas yield | Activation energies (kcal/mol) | Fractional gas yield |
| 65.4 | 0.0000 | 65.2 | 0.0008 | 64.9 | 0.0000 | 65.0 | 0.0000 |
| 64.4 | 0.0000 | 64.2 | 0.0025 | 63.9 | 0.0000 | 64.0 | 0.0007 |
| 63.4 | 0.0000 | 63.2 | 0.0064 | 62.9 | 0.0009 | 63.0 | 0.0021 |
| 62.4 | 0.0000 | 62.2 | 0.0145 | 61.9 | 0.0023 | 62.0 | 0.0057 |
| 61.4 | 0.0000 | 61.2 | 0.0292 | 60.9 | 0.0052 | 61.0 | 0.0134 |
| 60.4 | 0.0000 | 60.2 | 0.0515 | 59.9 | 0.0110 | 60.0 | 0.0278 |
| 59.4 | 0.0000 | 59.2 | 0.0803 | 58.9 | 0.0211 | 59.0 | 0.0504 |
| 58.4 | 0.0000 | 58.2 | 0.1102 | 57.9 | 0.0363 | 58.0 | 0.0800 |
| 57.4 | 0.0000 | 57.2 | 0.1333 | 56.9 | 0.0568 | 57.0 | 0.1114 |
| 56.4 | 0.0000 | 56.2 | 0.1420 | 55.9 | 0.0804 | 56.0 | 0.1358 |
| 55.4 | 0.0000 | 55.2 | 0.1333 | 54.9 | 0.1031 | 55.0 | 0.1451 |
| 54.4 | 0.0000 | 54.2 | 0.1102 | 53.9 | 0.1196 | 54.0 | 0.1358 |
| 53.4 | 0.0000 | 53.2 | 0.0803 | 52.9 | 0.1257 | 53.0 | 0.1114 |
| 52.4 | 0.0000 | 52.2 | 0.0515 | 51.9 | 0.1196 | 52.0 | 0.0800 |
| 51.4 | 0.0000 | 51.2 | 0.0292 | 50.9 | 0.1031 | 51.0 | 0.0504 |
| 50.4 | 0.0000 | 50.2 | 0.0145 | 49.9 | 0.0804 | 50.0 | 0.0278 |
| 49.4 | 0.0000 | 49.2 | 0.0064 | 48.9 | 0.0568 | 49.0 | 0.0134 |
| 48.4 | 0.0012 | 48.2 | 0.0025 | 47.9 | 0.0363 | 48.0 | 0.0057 |
| 47.4 | 0.0329 | 47.2 | 0.0008 | 46.9 | 0.0211 | 47.0 | 0.0021 |
| 46.4 | 0.2370 | 46.2 | 0.0000 | 45.9 | 0.0110 | 46.0 | 0.0007 |
| 45.4 | 0.4577 | 45.2 | 0.0000 | 44.9 | 0.0052 | 45.0 | 0.0000 |
| 44.4 | 0.2370 | 44.2 | 0.0000 | 43.9 | 0.0023 | 44.0 | 0.0000 |
| 43.4 | 0.0329 | 43.2 | 0.0000 | 42.9 | 0.0009 | 43.0 | 0.0000 |
| 42.4 | 0.0012 | 42.2 | 0.0000 | 41.9 | 0.0000 | 42.0 | 0.0000 |
| Frequency factor (1/m.y.) | 7.88E+23 | | 1.23E+28 | | 5.68E+26 | | 3.15E+27 |

As a result, the gas-generation curve of the St. Medard (SM) source rock serves as a representative average for this anhydrous-pyrolysis model (table 6). At the top of the deep gas depth (15,000 feet/4,572 m), 35 percent of gas generation from oil retained in a source rock is completed at 1°C/m.y. Therefore 65 mg/g C of deep gas is generated (fig. 6*A* and table 6). This model predicts that the deep gas generation is finished (that is, $X$=0.99) at a depth of 21,654 feet (6,600 m) (table 6). At the top of the deep-gas depth (15,000 feet/4,572 m), this model predicts 100 percent of gas generation from oil retained in a mature

**Table 5.** Maximum $C_1$–$C_5$ gas yields for different starting materials used in six kinetic models.

| Starting material | Model reference* | Maximum gas yield (mg/g C) |
|---|---|---|
| Type-I kerogen | 1 | 88.5 |
| | 2 | 78.0 |
| Type-II kerogen | 1 | 70.0 |
| | 2 | 100.6 |
| | 3 | **92.8 |
| Type-IIS kerogen | 1 | 70.3 |
| | 2 | 104.9 |
| Type-III kerogen | 1 | 57.1 |
| | 2 | 76.6 |
| Type-III' kerogen | 1 | 54.2 |
| | 2 | 69.5 |
| Source-rock oil | 4 | 100.0 |
| Reservoir oil | 5 | 541.2 |
| | *(mg/g oil)* | *(460.0)* |
| | 6 | 376.2 |
| | *(mg/g oil)* | *(319.8)* |

* References: 1, Behar and others (1997); 2, Pepper and Corvi (1995); 3, Knauss and others (1997); 4, Pepper and Dodd (1995); 5, Horsfield and others (1992); 6, Tsuzuki and others (1997).

**$C_1$–$C_4$

source rock completed at 10°C/m.y. Therefore, according to this model, essentially no deep gas is generated from oil retained in a source rock at this heating rate.

### Reservoir Oil to Gas

Generation of gas from the cracking of oil in reservoirs is considered by the anhydrous- and hydrous-pyrolysis models by Horsfield and others (1992) and Tsuzuki and others (1997), respectively. Figure 7 shows the gas generation curves for reservoir-oil cracking in basins with 1° and 10°C/m.y. heating rates as predicted by the anhydrous- and hydrous-pyrolysis models. At the top of the deep gas depth (15,000 feet/4,572 m), 2 and 0 percent of gas generation from reservoir-oil cracking are completed at 1°C/m.y., according to the anhydrous- and hydrous-pyrolysis models, respectively. Therefore, 449.5 and 320.2 mg/g oil of deep gas are generated according to the closed anhydrous- and hydrous-pyrolysis models, respectively (fig. 7*A* and table 6). These models predict that the deep gas generation is finished (that is, $X$=0.99) at depths of 24,934 and 24,278 feet (7,600 and 7,400 m) (table 6). At the top of the deep gas depth (15,000 feet/4,572 m), the anhydrous- and hydrous-pyrolysis models predict 80 and 53 percent of gas generation from reservoir-oil cracking completed at 10°C/m.y., respectively. According to these models at 10°C/m.y., 459.6 and 320.2 mg/g oil of deep gas are generated from reservoir oil cracking when reservoirs reach depths of 13,780 and 17,060 feet (4,200 and 5,200 m), respectively.

## Discussion

### Kerogen to Gas

Gas generation from kerogen at deep depths is more likely at slow basin heating rates irrespective of kerogen type or kinetic model (table 7). At the slow heating rate of 1°C/m.y., 5–75 mg/g C of deep gas can be generated irrespective of kerogen type or kinetic model. In contrast, at the fast heating rate of 10°C/m.y., only 0–15 mg/g C of deep gas are generated irrespective of kerogen type or kinetic model (table 7). The implication here is that only a finite amount of gas can be generated from kerogen within a specific thermal-stress interval. Slow heating rates result in lower temperatures at greater depths, which allows this thermal-stress interval to be extended to greater depths within a basin. Therefore, according to these models, deep basins with cooler subsurface temperatures are more likely to generate deep gas from kerogen than deep basins with hotter subsurface temperatures.

For the slow heating rate, the composite-pyrolysis model predicts the greatest amount of deep gas, with values ranging from 5 to 75 mg/g C (table 7). The open-pyrolysis model gives a lower value for deep gas generation, from 8 to 51 mg/g C (table 7). However, at the rapid heating rate, the open-pyrolysis model predicts greater amounts (1–15 mg/g C) of deep gas generation than that predicted by the composite-pyrolysis model (0–7 mg/g C). The hydrous-pyrolysis model for only Type-II kerogen yields no deep gas at the high heating rate and 23 mg/g C of deep gas at the slow heating rate. Obviously, more hydrous-pyrolysis kinetic studies on the other kerogen types are needed.

It would be valuable to compare all the different kerogen types for the three pyrolysis models, but a complete comparison of kerogen types is only possible between the open- and composite-pyrolysis models. At both heating rates, the open-pyrolysis model predicts an increase in the amount of deep gas generated from Type-I to Type-II to Type-III kerogen. With the exception of Type-IIS kerogen, this trend is also predicted by the composite-pyrolysis model (that is, Type-I < Type-II < Type-III kerogen). The composite-pyrolysis method predicts that Type-IIS kerogen generates the least amount of deep gas at both heating rates. The implication of this prediction is that deep basins with high-sulfur oils and carbonate source rocks are not good prospects for deep gas. However, in the open-pyrolysis model, Type-IIS kerogen generates about the same amount of deep gas as Type-II kerogen at both heating rates.

For the slow heating rate, the composite-pyrolysis model predicts more deep gas generation than the open-pyrolysis model for all kerogen types except for Type-IIS kerogen. As an

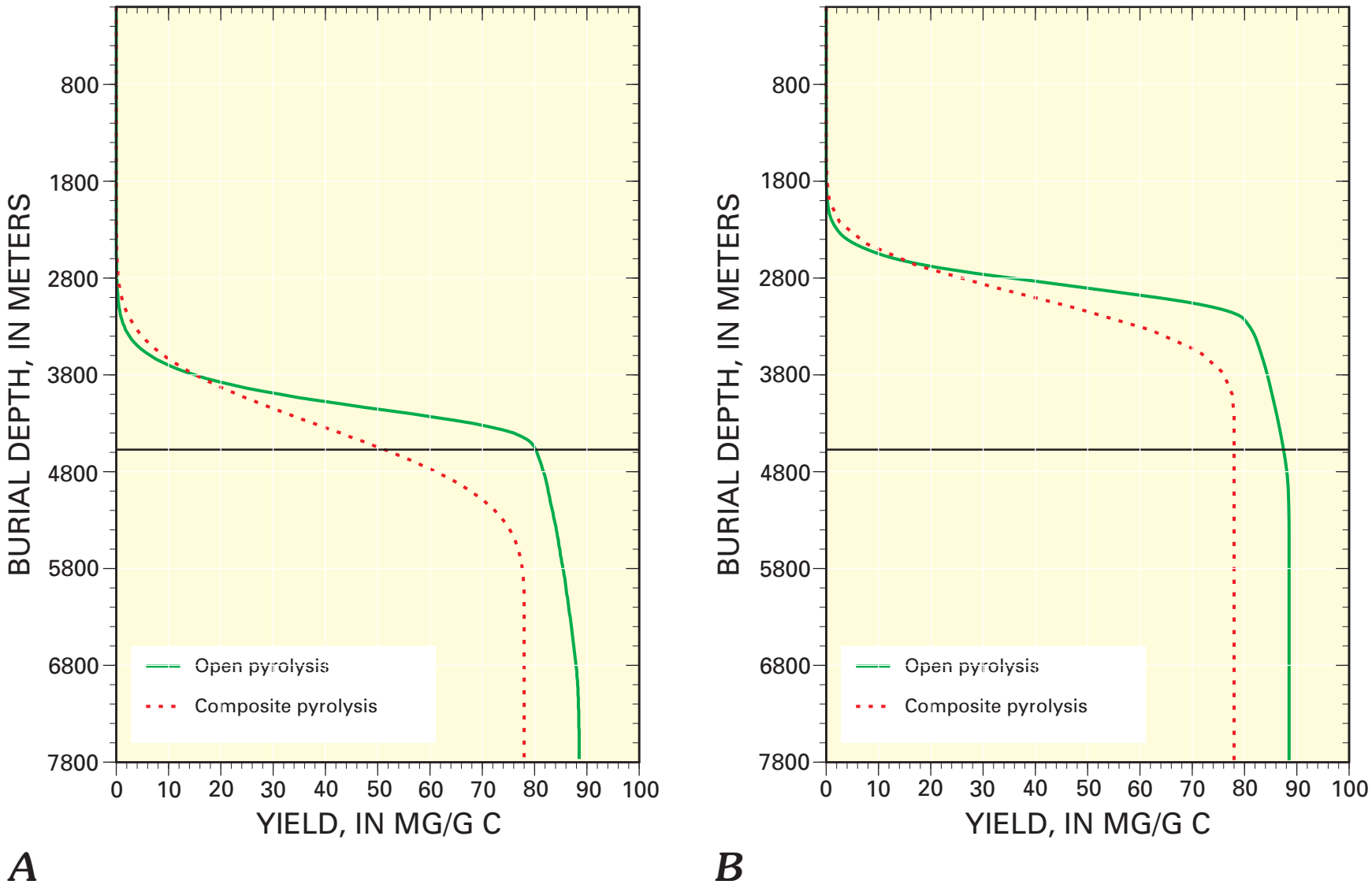


**Figure 1.** Amount of $C_1$–$C_5$ gas generated from Type-I kerogen with increasing burial depth, according to open-pyrolysis (solid line; Behar and others, 1997) and composite-pyrolysis (dotted line; Pepper and Corvi, 1995) models at geologic heating rates of *A*, 1°C/m.y., and *B*, 10°C/m.y. Deep gas depths occur below solid horizontal line drawn at 15,000 feet/4,572 m.

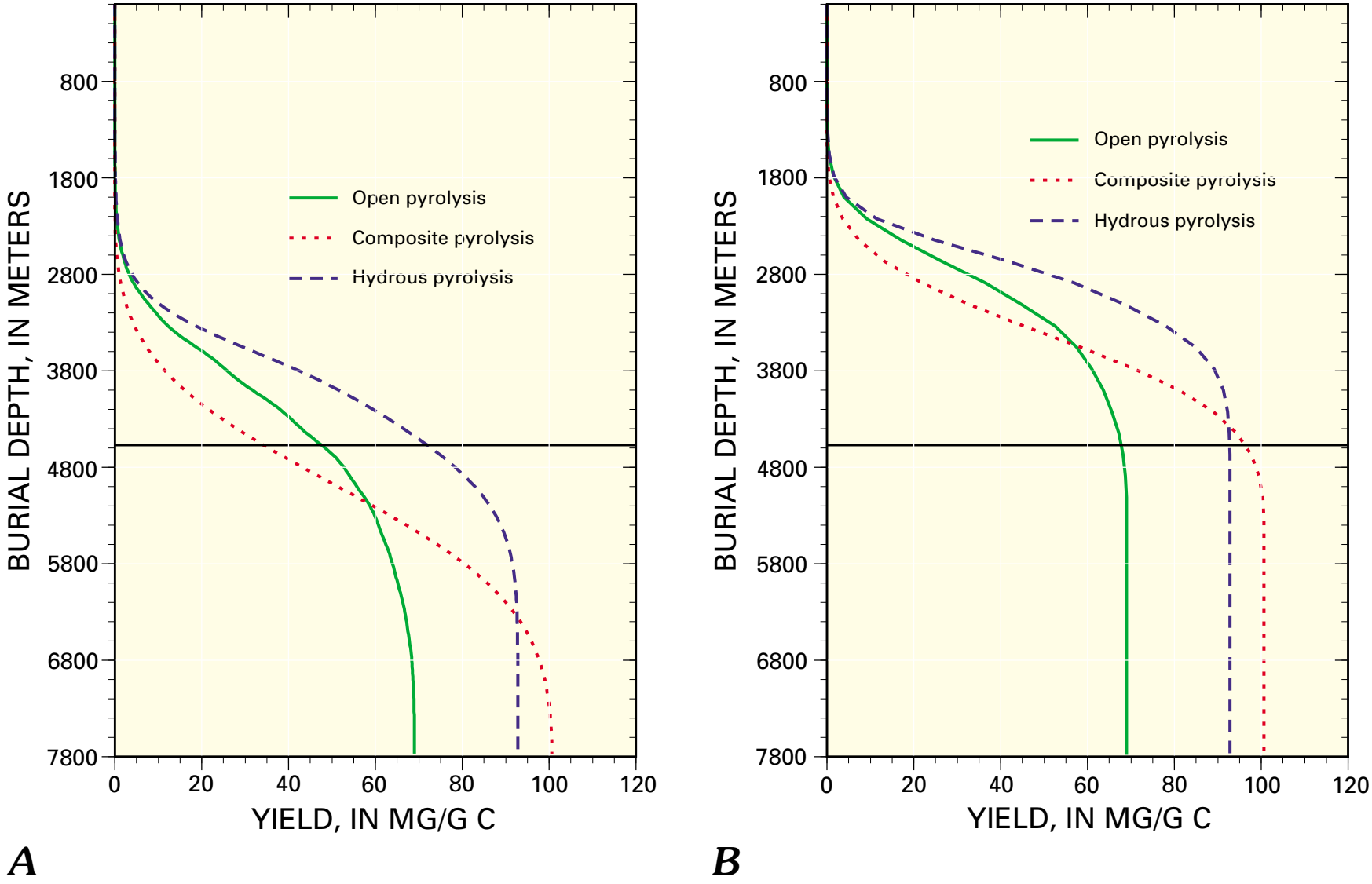


**Figure 2.** Amount of gas generated from Type-II kerogen with increasing burial depth, according to open-pyrolysis (solid line; $C_1$–$C_5$; Behar and others, 1997), composite-pyrolysis (dotted line; $C_1$–$C_5$; Pepper and Corvi, 1995), and hydrous-pyrolysis (dashed line; $C_1$–$C_4$; Knauss and others, 1997) models at geologic heating rates of *A*, 1°C/m.y., and *B*, 10°C/m.y. Deep gas depths occur below solid horizontal line drawn at 15,000 feet/4,572 m.

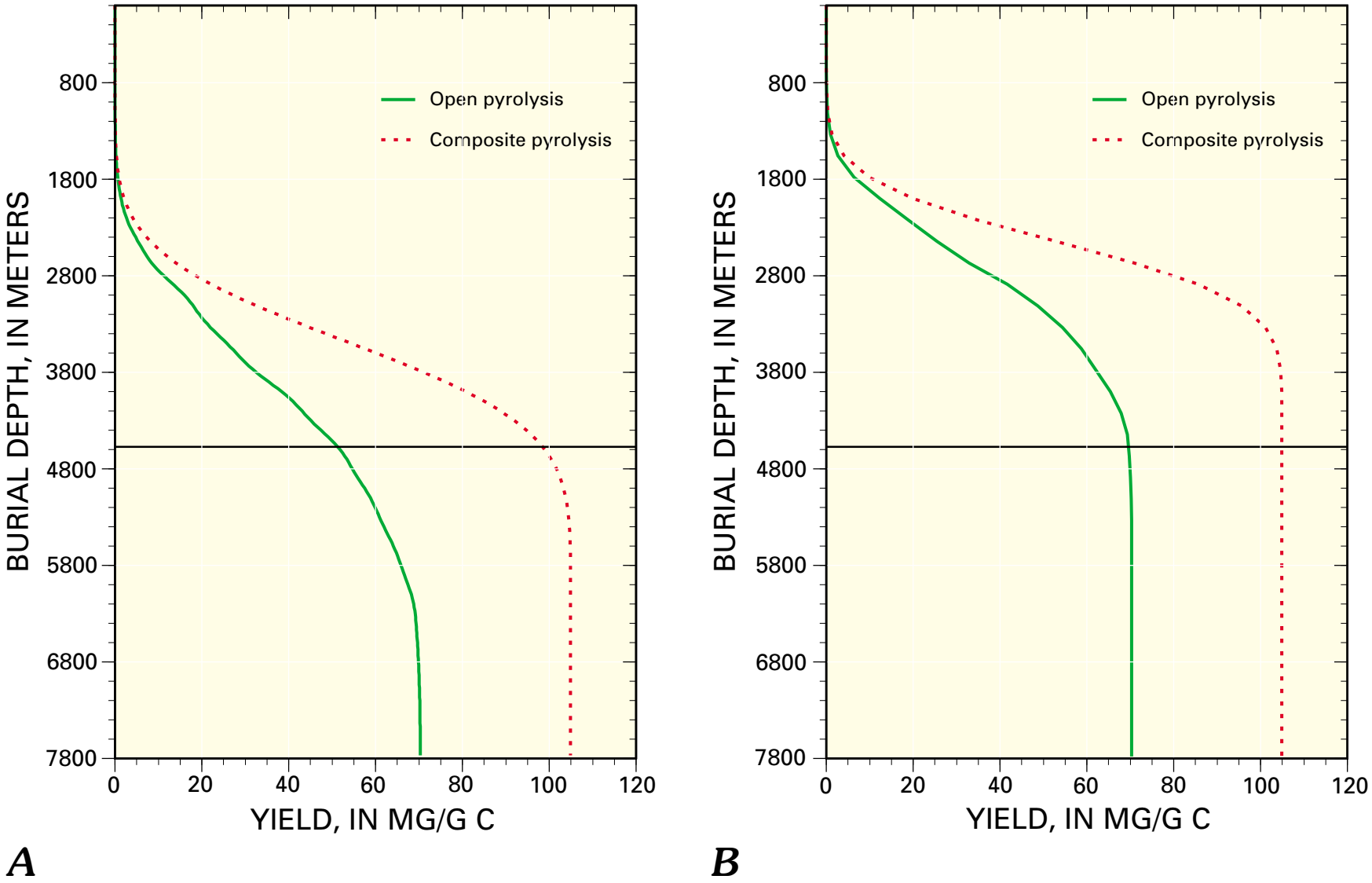


**Figure 3.** Amount of $C_1$–$C_5$ gas generated from Type-IIS kerogen with increasing burial depth, according to open-pyrolysis (solid line; Behar and others, 1997) and composite-pyrolysis (dotted line; Pepper and Corvi, 1995) models at geologic heating rates of *A*, 1°C/m.y., and *B*, 10°C/m.y. Deep gas depths occur below horizontal line drawn at 15,000 feet/4,572 m.

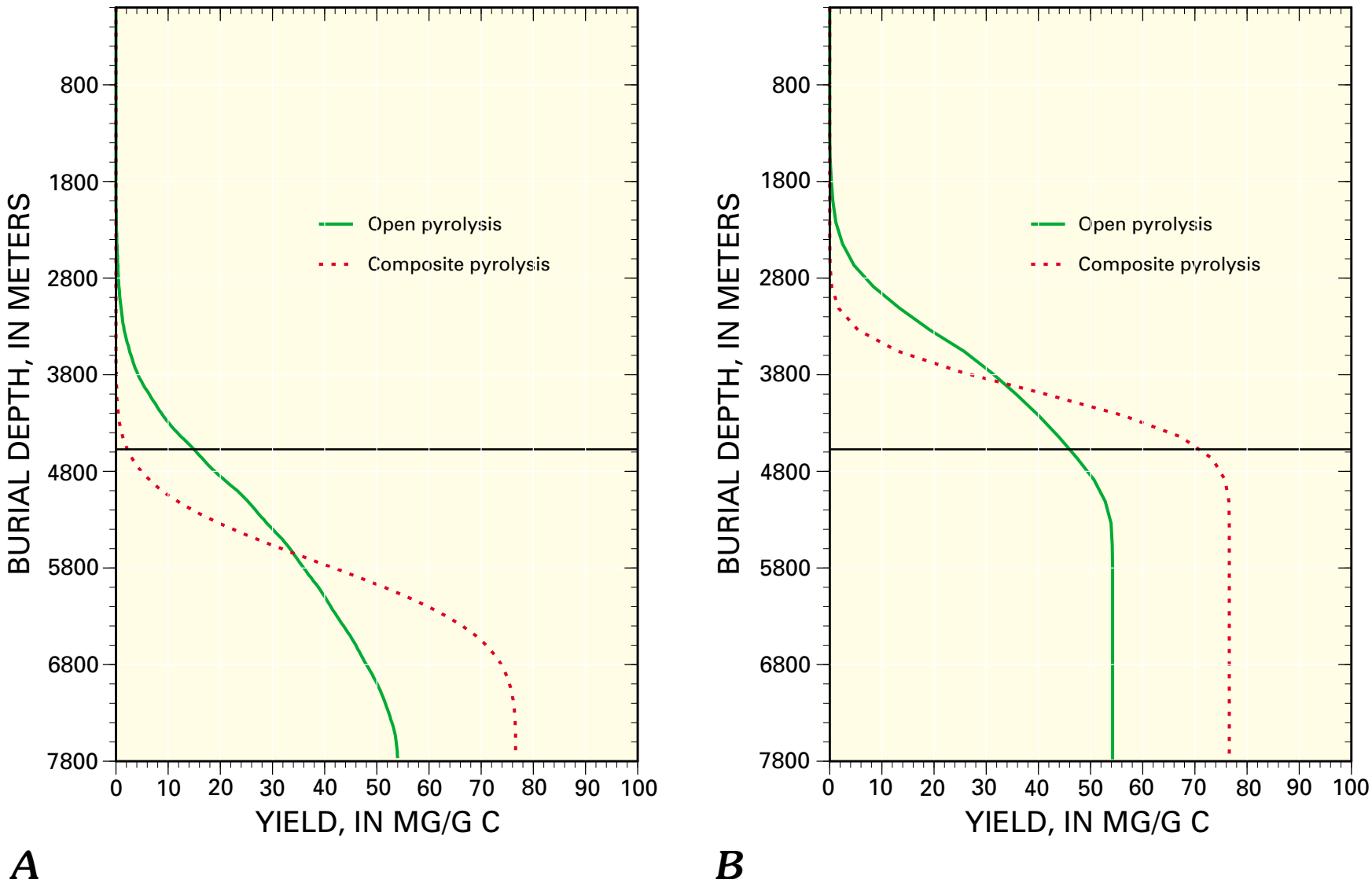


**Figure 4.** Amount of $C_1$–$C_5$ gas generated from Type-III kerogen with increasing burial depth, according to open-pyrolysis (solid line; Behar and others, 1997) and composite-pyrolysis (dotted line; Pepper and Corvi, 1995) models at geologic heating rates of *A*, 1°C/m.y., and *B*, 10°C/m.y. Deep gas depths occur below horizontal line drawn at 15,000 feet/4,572 m.

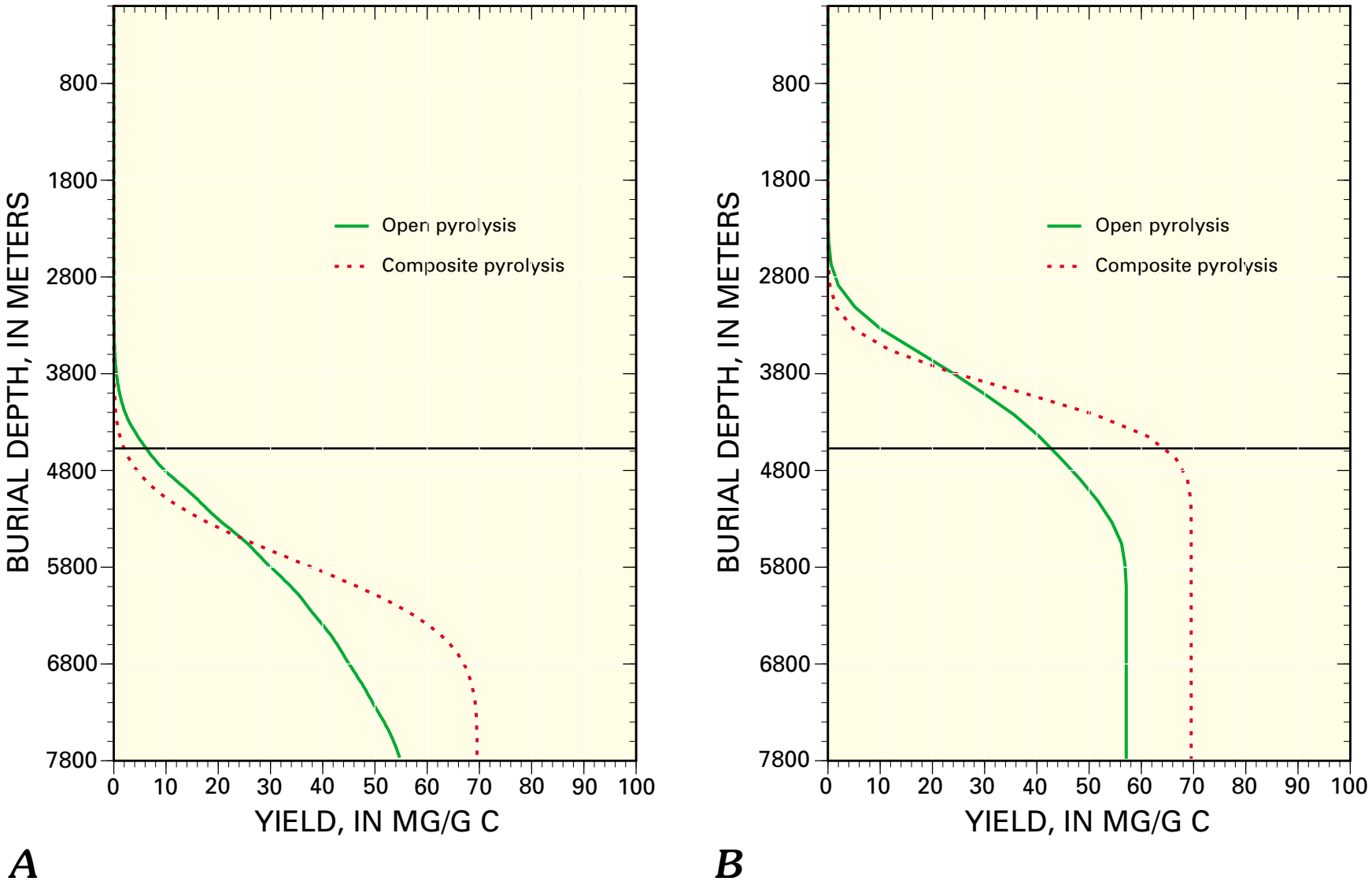


**Figure 5.** Amount of $C_1$–$C_5$ gas generated from Type-III′ (paraffinic) kerogen with increasing burial depth, according to open-pyrolysis (solid line; Behar and others, 1997) and composite-pyrolysis (dotted line; Pepper and Corvi, 1995) models at geologic heating rates of *A*, 1°C/m.y., and *B*, 10°C/m.y. Deep gas depths occur below horizontal line drawn at 15,000 feet/4,572 m.

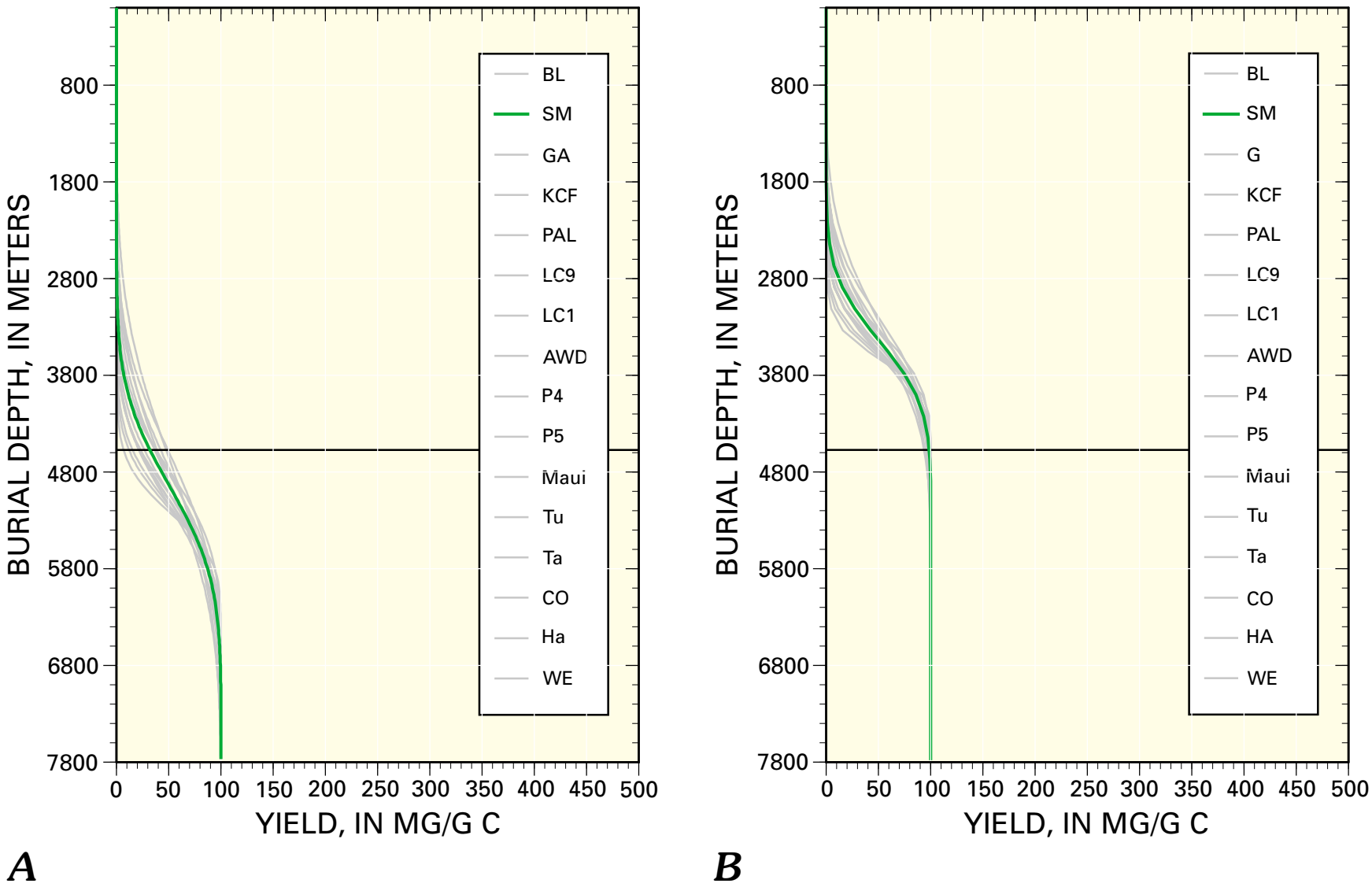


**Figure 6.** Amount of $C_1$–$C_5$ gas generated from the cracking of oil in 16 different source rocks with increasing burial depth, according to anhydrous-pyrolysis model (solid lines; Pepper and Corvi, 1995) at geologic heating rates of *A*, 1°C/m.y., and *B*, 10°C/m.y. Deep gas depths occur below horizontal line drawn at 15,000 feet/4,572 m. BL, Brown Limestone; SM, St. Medard; GA, Garlin; KCF, not given; PAL, not given; LC9, LC995; LC1, LC1005; AWD, not given; P4, Pematang 45.2; P5, Pematang 52.7; Maui, Maui; Tu, Tuna; Ta, Tarakan; CO, COST; Ha, Haltenbanken; and WE, Westfield. Bold-solid St. Medard (SM) curve was selected to be the single representative gas generation curve for all 16 samples.

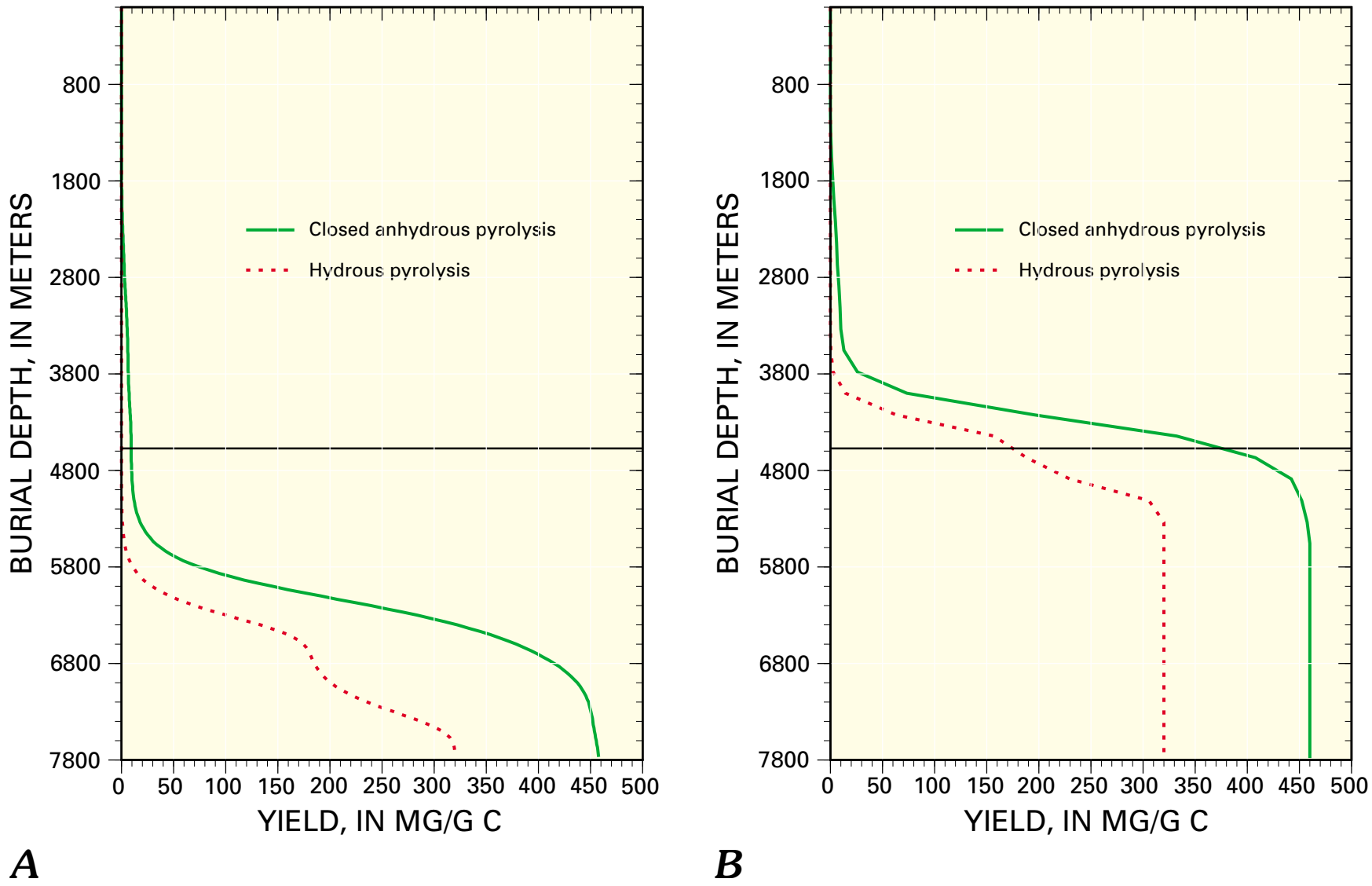


**Figure 7.** Amount of gas generated from the cracking of reservoir oil with increasing burial depth, according to anhydrous-pyrolysis model (solid line; $C_1$–$C_4$; Horsfield and others, 1992) and hydrous-pyrolysis (dotted line; $C_1$–$C_4$; Tsuzuki and others, 1997) models at geologic heating rates of *A*, 1°C/m.y., and *B*, 10°C/m.y. Deep gas depths occur below horizontal line drawn at 15,000 feet/4,572 m.

**Table 6.** Summary of gas generation curves for kerogens and oils (figs. 1–6) with respect to yield, depth, time, and temperature for fraction of reaction values of 0.05, 0.25, 0.50, 0.75, and 0.99 at 1° and 10°C/m.y. heating rates for each kinetic model.

[Last column of each heating rate gives the fraction of reaction, yield, time, and temperature at the start of deep gas (15,000 feet—4,572 m)]

| | 1°C/m.y. | | | | | | 10°C/m.y. | | | | | |
|---|---|---|---|---|---|---|---|---|---|---|---|---|
| **Type-I kerogen** | | | | | | | | | | | | |
| Open-pyrolysis model[1] | | | | | | | | | | | | |
| Fraction of reaction (X) | 0.050 | 0.250 | 0.500 | 0.750 | 0.990 | 0.909 | 0.050 | 0.250 | 0.500 | 0.750 | 0.990 | 0.989 |
| Gas yield (mg/g C) | 4 | 22 | 44 | 66 | 87 | 80 | 4 | 22 | 44 | 66 | 87 | 87 |
| ($ft^3$/kg C) | 0.168 | 0.840 | 1.680 | 2.520 | 3.326 | 3.054 | 0.168 | 0.840 | 1.680 | 2.520 | 3.326 | 3.321 |
| Depth (m) | 3600 | 4000 | 4200 | 4200 | 6800 | 4572 | 2400 | 2600 | 2800 | 3000 | 4572 | 4572 |
| Time (m.y.) | 108 | 120 | 126 | 126 | 204 | 137 | 11 | 12 | 13 | 14 | 21 | 21 |
| Temperature (°C) | 128 | 140 | 146 | 146 | 224 | 157 | 128 | 137 | 146 | 155 | 226 | 226 |
| Composite-pyrolysis model[2] | | | | | | | | | | | | |
| Fraction of reaction (X) | 0.050 | 0.250 | 0.500 | 0.750 | 0.990 | 0.641 | 0.050 | 0.250 | 0.500 | 0.750 | 0.990 | 1.000 |
| Gas yield (mg/g C) | 4 | 20 | 39 | 59 | 77 | 78 | 4 | 20 | 39 | 59 | 77 | 78 |
| ($ft^3$/kg C) | 0.149 | 0.744 | 1.489 | 2.233 | 2.948 | 2.978 | 0.149 | 0.744 | 1.489 | 2.233 | 2.948 | 2.978 |
| Depth (m) | 3400 | 4000 | 4400 | 4800 | 5600 | 4572 | 2400 | 2600 | 3000 | 3400 | 4000 | 4572 |
| Time (m.y.) | 102 | 120 | 132 | 144 | 168 | 137 | 11 | 12 | 14 | 15 | 18 | 21 |
| Temperature (°C) | 122 | 140 | 152 | 164 | 188 | 157 | 128 | 137 | 155 | 173 | 200 | 226 |
| **Type-II kerogen** | | | | | | | | | | | | |
| Open-pyrolysis model[1] | | | | | | | | | | | | |
| Fraction of reaction (X) | 0.050 | 0.250 | 0.500 | 0.750 | 0.990 | 0.671 | 0.050 | 0.250 | 0.500 | 0.750 | 0.990 | 0.971 |
| Gas yield (mg/g C) | 4 | 18 | 35 | 53 | 69 | 47 | 4 | 18 | 35 | 53 | 69 | 68 |
| ($ft^3$/kg C) | 0.134 | 0.668 | 1.336 | 2.004 | 2.645 | 1.794 | 0.134 | 0.668 | 1.336 | 2.004 | 2.645 | 2.596 |
| Depth (m) | 2800 | 3600 | 4200 | 4800 | 6800 | 4572 | 1800 | 2400 | 2800 | 3200 | 4800 | 4572 |
| Time (m.y.) | 84 | 108 | 126 | 144 | 204 | 137 | 8 | 11 | 13 | 14 | 22 | 21 |
| Temperature (°C) | 104 | 128 | 146 | 164 | 224 | 157 | 101 | 128 | 146 | 164 | 236 | 226 |
| Composite-pyrolysis model[2] | | | | | | | | | | | | |
| Fraction of reaction (X) | 0.050 | 0.250 | 0.500 | 0.750 | 0.990 | 0.350 | 0.050 | 0.250 | 0.500 | 0.750 | 0.990 | 0.950 |
| Gas yield (mg/g C) | 5 | 25 | 50 | 75 | 99 | 35 | 5 | 25 | 50 | 75 | 99 | 95 |
| ($ft^3$/kg C) | 0.191 | 0.954 | 1.909 | 2.863 | 3.779 | 1.336 | 0.191 | 0.954 | 1.909 | 2.863 | 3.779 | 3.627 |
| Depth (m) | 3400 | 4400 | 5000 | 5600 | 7200 | 4572 | 2400 | 3000 | 3400 | 3800 | 5000 | 4572 |
| Time (m.y.) | 102 | 132 | 150 | 168 | 216 | 137 | 11 | 14 | 15 | 17 | 23 | 21 |
| Temperature (°C) | 122 | 152 | 170 | 188 | 236 | 157 | 128 | 155 | 173 | 191 | 245 | 226 |
| Hydrous-pyrolysis model[3] | | | | | | | | | | | | |
| Fraction of reaction (X) | 0.050 | 0.250 | 0.500 | 0.750 | 0.990 | 0.753 | 0.050 | 0.250 | 0.500 | 0.750 | 0.990 | 1.000 |
| Gas yield (mg/g C) | 5 | 23 | 47 | 70 | 92 | 70 | 5 | 23 | 47 | 70 | 92 | 93 |
| ($ft^3$/kg C) | 0.180 | 0.899 | 1.797 | 2.696 | 3.559 | 2.706 | 0.180 | 0.899 | 1.797 | 2.696 | 3.559 | 3.595 |
| Depth (m) | 2800 | 3400 | 3800 | 4572 | 5800 | 4572 | 2000 | 2400 | 2800 | 3200 | 4000 | 4572 |
| Time (m.y.) | 84 | 102 | 114 | 137 | 174 | 137 | 9 | 11 | 13 | 14 | 18 | 21 |
| Temperature (°C) | 104 | 122 | 134 | 157 | 194 | 157 | 110 | 128 | 146 | 164 | 200 | 226 |

**Table 6—Continued.** Summary of gas generation curves for kerogens and oils (figs. 1–6) with respect to yield, depth, time, and temperature for fraction of reaction values of 0.05, 0.25, 0.50, 0.75, and 0.99 at 1° and 10°C/m.y. heating rates for each kinetic model.

[Last column of each heating rate gives the fraction of reaction, yield, time, and temperature at the start of deep gas (15,000 feet—4,572 m)]

| | 1°C/m.y. | | | | | | 10°C/m.y. | | | | | |
|---|---|---|---|---|---|---|---|---|---|---|---|---|
| **Type-IIS kerogen** | | | | | | | | | | | | |
| Open-pyrolysis model[1] | | | | | | | | | | | | |
| Fraction of reaction (X) | 0.050 | 0.250 | 0.500 | 0.750 | 0.990 | 0.743 | 0.050 | 0.250 | 0.500 | 0.750 | 0.990 | 0.986 |
| Gas yield (mg/g C) | 4 | 18 | 35 | 53 | 69 | 52 | 4 | 18 | 35 | 53 | 69 | 69 |
| ($ft^3$/kg C) | 0.134 | 0.668 | 1.336 | 2.004 | 2.645 | 1.985 | 0.134 | 0.668 | 1.336 | 2.004 | 2.645 | 2.634 |
| Depth (m) | 2400 | 3000 | 4000 | 4572 | 6400 | 4572 | 1600 | 2200 | 2800 | 3200 | 4572 | 4572 |
| Time (m.y.) | 72 | 90 | 120 | 137 | 192 | 137 | 7 | 10 | 13 | 14 | 21 | 21 |
| Temperature (°C) | 92 | 110 | 140 | 157 | 212 | 157 | 92 | 119 | 146 | 164 | 226 | 226 |
| Composite-pyrolysis model[2] | | | | | | | | | | | | |
| Fraction of reaction (X) | 0.050 | 0.250 | 0.500 | 0.750 | 0.990 | 0.933 | 0.050 | 0.250 | 0.500 | 0.750 | 0.990 | 1.000 |
| Gas yield (mg/g C) | 5 | 26 | 53 | 79 | 104 | 98 | 5 | 26 | 53 | 79 | 104 | 105 |
| ($ft^3$/kg C) | 0.200 | 1.002 | 2.004 | 3.006 | 3.968 | 3.741 | 0.200 | 1.002 | 2.004 | 3.006 | 3.968 | 4.008 |
| Depth (m) | 2400 | 3000 | 3400 | 4000 | 5000 | 4572 | 1600 | 2000 | 2400 | 2800 | 3600 | 4572 |
| Time (m.y.) | 72 | 90 | 102 | 120 | 150 | 137 | 7 | 9 | 11 | 13 | 16 | 21 |
| Temperature (°C) | 92 | 110 | 122 | 140 | 170 | 157 | 92 | 110 | 128 | 146 | 182 | 226 |
| **Type-III kerogen** | | | | | | | | | | | | |
| Open-pyrolysis model[1] | | | | | | | | | | | | |
| Fraction of reaction (X) | 0.050 | 0.250 | 0.500 | 0.750 | 0.990 | 0.259 | 0.050 | 0.250 | 0.500 | 0.750 | 0.990 | 0.852 |
| Gas yield (mg/g C) | 3 | 14 | 27 | 41 | 53 | 14 | 3 | 14 | 27 | 41 | 53 | 46 |
| ($ft^3$/kg C) | 0.000103 | 0.000515 | 0.001031 | 0.001546 | 0.002041 | 0.000534 | 0.000103 | 0.000515 | 0.001031 | 0.001546 | 0.002041 | 0.001756 |
| Depth (m) | 3600 | 4400 | 5200 | 6200 | 7400 | 4572 | 2400 | 3200 | 3600 | 4200 | 5200 | 4572 |
| Time (m.y.) | 108 | 132 | 156 | 186 | 222 | 137 | 11 | 14 | 16 | 19 | 23 | 21 |
| Temperature (°C) | 128 | 152 | 176 | 206 | 242 | 157 | 128 | 164 | 182 | 209 | 254 | 226 |
| Composite-pyrolysis model[2] | | | | | | | | | | | | |
| Fraction of reaction (X) | 0.050 | 0.250 | 0.500 | 0.750 | 0.990 | 0.026 | 0.050 | 0.250 | 0.500 | 0.750 | 0.990 | 0.921 |
| Gas yield (mg/g C) | 4 | 19 | 38 | 57 | 75 | 2 | 4 | 19 | 38 | 57 | 75 | 70 |
| ($ft^3$/kg C) | 0.145 | 0.725 | 1.451 | 2.176 | 2.872 | 0.076 | 0.145 | 0.725 | 1.451 | 2.176 | 2.872 | 2.672 |
| Depth (m) | 4800 | 5400 | 5800 | 6000 | 7000 | 4572 | 3200 | 3600 | 4000 | 4200 | 4800 | 4572 |
| Time (m.y.) | 144 | 162 | 174 | 180 | 210 | 137 | 14 | 16 | 18 | 19 | 22 | 21 |
| Temperature (°C) | 164 | 182 | 194 | 200 | 230 | 157 | 164 | 182 | 200 | 209 | 236 | 226 |
| **Type-III' kerogen** | | | | | | | | | | | | |
| Open-pyrolysis model[1] | | | | | | | | | | | | |
| Fraction of reaction (X) | 0.050 | 0.250 | 0.500 | 0.750 | 0.990 | 0.105 | 0.050 | 0.250 | 0.500 | 0.750 | 0.990 | 0.737 |
| Gas yield (mg/g C) | 3 | 14 | 29 | 43 | 56 | 6 | 3 | 14 | 29 | 43 | 56 | 42 |
| ($ft^3$/kg C) | 0.109 | 0.544 | 1.088 | 1.632 | 2.154 | 0.229 | 0.109 | 0.544 | 1.088 | 1.632 | 2.154 | 1.603 |
| Depth (m) | 4200 | 5000 | 5800 | 6600 | 7800 | 4572 | 3000 | 3400 | 4000 | 4572 | 5600 | 4572 |
| Time (m.y.) | 126 | 150 | 174 | 198 | 234 | 137 | 14 | 15 | 18 | 21 | 25 | 21 |
| Temperature (°C) | 146 | 170 | 194 | 218 | 254 | 157 | 155 | 173 | 200 | 226 | 272 | 226 |

**Table 6—Continued.** Summary of gas generation curves for kerogens and oils (figs. 1–6) with respect to yield, depth, time, and temperature for fraction of reaction values of 0.05, 0.25, 0.50, 0.75, and 0.99 at 1° and 10°C/m.y. heating rates for each kinetic model.

[Last column of each heating rate gives the fraction of reaction, yield, time, and temperature at the start of deep gas (15,000 feet—4,572 m)]

| **Type-III' kerogen** | 1°C/m.y. | | | | | | 10°C/m.y. | | | | | |
|---|---|---|---|---|---|---|---|---|---|---|---|---|
| Composite-pyrolysis model [2] | | | | | | | | | | | | |
| Fraction of reaction (X) | 0.050 | 0.250 | 0.500 | 0.750 | 0.990 | 0.029 | 0.050 | 0.250 | 0.500 | 0.750 | 0.990 | 0.914 |
| Gas yield (mg/g C) | 4 | 18 | 35 | 53 | 69 | 2 | 4 | 18 | 35 | 53 | 69 | 64 |
| ($ft^3$/kg C) | 0.134 | 0.668 | 1.336 | 2.004 | 2.645 | 0.076 | 0.134 | 0.668 | 1.336 | 2.004 | 2.645 | 2.443 |
| Depth (m) | 4600 | 5400 | 5800 | 6000 | 7000 | 4572 | 3200 | 3600 | 4000 | 4200 | 4800 | 4572 |
| Time (m.y.) | 138 | 162 | 174 | 180 | 210 | 137 | 14 | 16 | 18 | 19 | 22 | 21 |
| Temperature (°C) | 158 | 182 | 194 | 200 | 230 | 157 | 164 | 182 | 200 | 209 | 236 | 226 |
| **Oil in source rock** | | | | | | | | | | | | |
| Anhydrous-pyrolysis model [4] | | | | | | | | | | | | |
| Fraction of reaction (X) | 0.050 | 0.250 | 0.500 | 0.750 | 0.990 | 0.353 | 0.050 | 0.250 | 0.500 | 0.750 | 0.990 | 1.000 |
| Gas yield (mg/g C) | 5 | 25 | 50 | 75 | 99 | 35 | 5 | 25 | 50 | 75 | 99 | 100 |
| ($ft^3$/kg C) | 0.191 | 0.954 | 1.909 | 2.863 | 3.779 | 1.347 | 0.191 | 0.954 | 1.909 | 2.863 | 3.779 | 3.817 |
| Depth (m) | 3600 | 4400 | 5000 | 5400 | 6600 | 4572 | 2400 | 3000 | 3400 | 3800 | 4200 | 4572 |
| Time (m.y.) | 108 | 132 | 150 | 162 | 198 | 137 | 11 | 14 | 15 | 17 | 19 | 21 |
| Temperature (°C) | 128 | 152 | 170 | 182 | 218 | 157 | 128 | 155 | 173 | 191 | 209 | 226 |
| **Oil in reservoirs** | | | | | | | | | | | | |
| Anhydrous-pyrolysis model [5] | | | | | | | | | | | | |
| Fraction of reaction (X) | 0.050 | 0.250 | 0.500 | 0.750 | 0.990 | at 15,000 ft | 0.050 | 0.250 | 0.500 | 0.750 | 0.990 | at 15,000 ft |
| Gas yield (mg/g oil) | 23 | 115 | 230 | 345 | 455 | 0.022 | 23 | 115 | 230 | 345 | 455 | 0.804 |
| ($ft^3$/kg oil) | 0.889 | 4.445 | 8.890 | 13.336 | 17.603 | 0.001 | 0.889 | 4.445 | 8.890 | 13.336 | 17.603 | 0.031 |
| Depth (m) | 5400 | 6000 | 6200 | 6400 | 7600 | 4572 | 3800 | 4000 | 4200 | 4400 | 5000 | 4572 |
| Time (m.y.) | 162 | 180 | 186 | 192 | 228 | 137 | 17 | 18 | 19 | 20 | 23 | 21 |
| Temperature (°C) | 182 | 200 | 206 | 212 | 248 | 157 | 191 | 200 | 209 | 218 | 245 | 226 |
| Anhydrous-pyrolysis model [6] | | | | | | | | | | | | |
| Fraction of reaction (X) | 0.050 | 0.250 | 0.500 | 0.750 | 0.990 | 0.000 | 0.050 | 0.250 | 0.500 | 0.750 | 0.990 | 0.531 |
| Gas yield (mg/g oil) | 16 | 80 | 160 | 240 | 317 | 0.000 | 16 | 80 | 160 | 240 | 317 | 170.000 |
| ($ft^3$/kg oil) | 0.000611 | 0.003054 | 0.006108 | 0.009162 | 0.012094 | 0.000 | 0.000611 | 0.003054 | 0.006108 | 0.009162 | 0.012094 | 0.006490 |
| Depth (m) | 5800 | 6200 | 6400 | 7200 | 7400 | 4572 | 4000 | 4200 | 4400 | 5000 | 5200 | 4572 |
| Time (m.y.) | 174 | 186 | 192 | 216 | 222 | 137 | 18 | 19 | 20 | 23 | 23 | 21 |
| Temperature (°C) | 194 | 206 | 212 | 236 | 242 | 157 | 200 | 209 | 218 | 245 | 254 | 226 |

References: 1, Behar and others (1997); 2, Pepper and Corvi (1995); 3, Knauss and others (1997); 4, Pepper and Dodd (1995); 5, Horsfield and others (1992); 6, Tsuzuki and others (1997).

**Table 7.** Amounts of gas generated from kerogen above and below deep gas depth of 15,000 feet/4,572 m.

[All values refer to $C_1$–$C_5$ gas, except where otherwise noted]

| Kinetic model* | Kerogen type | 1°C/m.y. Gas generated | | 10°C/m.y. Gas generated | |
|---|---|---|---|---|---|
| | | Above 4,572 m (mg/g C) | Below 4,572 m (mg/g C) | Above 4,572 m (mg/g C) | Below 4,572 m (mg/g C) |
| Open pyrolysis[1] | Type-I | 80 | 8 | 87 | 1 |
| | Type-II | 50 | 20 | 68 | 2 |
| | Type-IIS | 50 | 20 | 69 | 1 |
| | Type-III | 6 | 51 | 42 | 15 |
| | Type-III' | 14 | 40 | 46 | 8 |
| Composite pyrolysis[2] | Type-I | 50 | 28 | 78 | 0 |
| | Type-II | 35 | 65 | 95 | 5 |
| | Type-IIS | 100 | 5 | 105 | 0 |
| | Type-III | 2 | 75 | 70 | 7 |
| | Type-III' | 2 | 68 | 64 | 6 |
| Hydrous pyrolysis[3] | Type-II | 70** | 23** | 93** | 0** |

*References: 1, Behar and others (1997); 2, Pepper and Corvi (1995); 3, Knauss and others (1997).

**All total gas is defined as $C_1$–$C_5$ except in these cases, where it is defined as $C_1$–$C_4$.

example, three times as much deep gas generation is predicted by Type-II kerogen in the composite-pyrolysis model than in the open-pyrolysis model. The hydrous-pyrolysis model for deep gas generation from Type-II kerogen predicts an intermediate value (23 mg/g C) at the low heating rate and the lowest value (0 mg/g C) at the high heating rate relative to the predictions by the composite- and open-pyrolysis models. Type-II kerogen is the most common source of oil, and the results presented here (table 7) suggest that the predicted potential for deep gas from this kerogen type is highly dependent on the pyrolysis model employed.

Type-I kerogen, which is typically associated with lacustrine sequences and source rocks, consistently has low yields of deep gas generation in both open- and composite-pyrolysis models and at both heating rates (table 7). These predictions suggest that basins with deeply buried lacustrine source rock sequences are not favorable for deep gas generation from kerogen. Conversely, Type-III kerogen produces more deep gas than the other kerogen types in both the open- and composite-pyrolysis models and for both heating rates. These predictions imply that basins with deeply buried coals are the most favorable for deep gas generation from kerogen.

## Oil to Gas

Deep gas from the cracking of oil retained in a source rock does not depend on kerogen type or lithology according to the anhydrous-pyrolysis model by Pepper and Dodd (1995). Similar to deep gas generation from kerogen, deep gas from retained oil in source rocks is most favorable at low heating rates (table 8). At 1°C/m.y., this model predicts amounts of deep gas generation that are comparable to those predicted by the composite-pyrolysis model for deep gas generation from Type-II and -III kerogens (table 8). At the high heating rate, no deep gas generation from the cracking of retained oil in source rocks is predicted (table 8). Therefore, at 10°C/m.y., deep gas generation from kerogen is more favorable than from the retained oil in a source rock.

Anhydrous- and hydrous-pyrolysis models predict that amounts of deep gas generated from the cracking of reservoir oil are 4–7 times greater at 1°C/m.y. and 6–20 times greater at 10°C/m.y. than the best deep gas yields obtained from kerogen (table 7). This difference is readily explained by the fact that oil has a higher thermal stability than kerogen. It has also been shown that the thermal stability of oil increases in the presence of liquid water (Hesp and Rigby, 1973), which would be ubiquitous in most subsurface reservoirs. This increase in stability with water is supported in part by the lower deep gas yields predicted by the hydrous-pyrolysis model than predicted by anhydrous-pyrolysis model at the high heating rate (table 6). Although the deep gas yields predicted for the cracking of reservoir oil are considerably higher than those for kerogen, the amount of kerogen in deeply buried source rocks of a sedimentary basin may be several orders of magnitude greater than the amounts of deeply buried reservoir oil.

**Table 8.** Amounts of gas generated from cracking of oil above and below deep gas depth of 15,000 feet/4,572 m.

[All values refer to $C_1$–$C_5$ gas, except where otherwise noted]

| Kinetic model* | Oil type | 1°C/m.y. Gas generated | | 10°C/m.y. Gas generated | |
|---|---|---|---|---|---|
| | | Above 4,572 m (mg/g C) | Below 4,572 m (mg/g C) | Above 4,572 m (mg/g C) | Below 4,572 m (mg/g C) |
| Source-rock oil | | | | | |
| Anhydrous pyrolysis[4] | Oil in source rock** | 29 | 71 | 100 | 0 |
| | | Gas generated | | Gas generated | |
| Reservoir oil | | Above 4,572 m (mg/g oil) | Below 4,572 m (mg/g oil) | Above 4,572 m (mg/g oil) | Below 4,572 m (mg/g oil) |
| Anhydrous pyrolysis[5] | North Sea (36° API) | 2** | 458** | 370** | 90** |
| Hydrous pyrolysis[6] | Sarukawa (33.6°API) | 0 | 320 | 170 | 150 |

*References: 4, Pepper and Dodd (1995); 5, Horsfield and others (1992); 6, Tsuzuki and others (1997).

**All total gas is defined as $C_1$–$C_5$ except in these cases, where it is defined as $C_1$–$C_4$.

## Conclusions and Future Studies

1. Basins with slow heating rates, where source rocks subside slowly through low thermal gradients, are more likely to yield deep gas from kerogen than basins with fast heating rates and rapid subsidence of source rock. Because this is one of the most important implications of this study, it would be interesting to compare amounts of deep gas and heating rates from different sedimentary basins. This would involve creating an inventory of heating rates for domestic basins as well as the amount of deep gas recovered to the present time. A future study of this type can be used to evaluate the validity of the different models used in this study and target basins with high potential for deep gas.

2. According to the open- and composite-pyrolysis models, Type-III kerogen will yield the most deep gas of the three kerogen types irrespective of heating rate. This implies that basins with deeply buried coals are most likely to contain deep gas. A future study comparing deep gas yields from basins with differing amounts of deeply buried coal would be a useful way of testing this model-based prediction and targeting basins with high potential for deep gas.

3. According to the open- and composite-pyrolysis models, Type-I kerogen has the least potential or no potential for deep gas generation. This implies that basins with deeply buried lacustrine source rocks are not likely to contain deep gas. A future study comparing deep gas yields from basins with differing amounts of deeply buried lacustrine source rocks would be a useful way of testing this model-based prediction and exclude basins with low potential for deep gas.

4. Cracking of reservoir oil is predicted by the anhydrous- and hydrous-pyrolysis models to generate the most deep gas irrespective of heating rate. Therefore, basins that currently have deeply buried overmature source rocks have the potential of previously having reservoir oil that has since cracked to generate deep gas. The main control for deep gas accumulations in this geologic setting is the original oil trap remaining competent with burial depth. The Gulf Coast offshore and the Anadarko basin may serve as examples of this geologic setting. Future studies of these types of basins can further elucidate the factors controlling deep gas accumulations and target other areas with high potential for deep gas.

5. No significant differences occur between the predicted amount of deep gas generated from kerogen by the different pyrolysis kinetic models. However, the hydrous-pyrolysis model considers only Type-II kerogen, and more hydrous-pyrolysis experiments with kinetic models for gas generation from Type-I, Type-IIS, and Type-III kerogens are needed to test this preliminary conclusion.

6. A significant difference occurs between the predicted amounts of deep gas generated from the cracking of reservoir oil by the anhydrous- and hydrous-pyrolysis kinetic models. The kinetic model derived from hydrous pyrolysis indicates that reservoir oil is more thermally stable and that oil cracking to gas requires higher thermal stress levels than those predicted by the anhydrous-pyrolysis model. More experimental work on the cracking of oil in the presence of water is needed. In addition, these future experiments need to consider the effects of commonly occurring reservoir minerals and their surfaces. Experiments published to 2000 on the cracking of reservoir oil have neglected the potential effects of minerals on gas generation.

## References Cited


Behar, F., and Vandenbroucke, M., 1996, Experimental determination of the rate constants of the *n*-$C_{25}$ thermal cracking at 120, 400, and 800 bar—Implications for high-pressure/high-temperature prospects: Energy & Fuels, v. 10, p. 932–940.

Behar, F., Vandenbroucke, M., Tang, Y., Marquis, F. and Espitalié, J., 1997, Thermal cracking of kerogen in open and closed systems—Determination of kinetic parameters and stoichiometric coefficients for oil and gas generation: Organic Geochemistry, v. 26, p. 321–339.

Braum, R.L., and Burnham, A.K., 1987, Analysis of chemical reactions using a distribution of activation energies and simpler models: Energy & Fuels, v. 1, p. 153–161.

Burnham, A.K., Gregg, H.R., Ward, R.L., Knauss, K.G., Copenhaver, S.A., Reynolds, J.G., and Sanborn, R., 1997, Decomposition kinetics and mechanism of *n*-hexadecane-1,2-$^{13}C_2$ and dodec-1-ene-1,2-$^{13}C_2$ doped in petroleum and *n*-hexadecane: Geochimica et Cosmochimica Acta, v. 61, pp. 3725–3737.

Domine, F., 1991, High pressure pyrolysis of *n*-hexane, 2,4-dimethylpentane and 1-phenylbutane—Is pressure an important geochemical parameter?: Organic Geochemistry, v. 17, p. 619–634.

Dyman, T.S., Rice, D.D., and Westcott, P.A., 1997, Introduction, *in* Dyman, T.S., Rice, D.D., and Westcott, P.A., eds., Geologic controls of deep natural gas resources in the United States: U.S. Geological Survey Bulletin 2146, p. 3–5.

Gorbachev, V.M., 1975, A solution to the exponential integral in the non-isothermal kinetics for linear heating: Journal of Thermal Analysis, v. 6, p. 349–350.

Gretener, P.E., and Curtis, C.D., 1982, Role of temperature and time on organic metamorphism: American Association of Petroleum Geologists Bulletin, v. 66, p. 1124–1129.

Hesp, W., and Rigby, D., 1973, The geochemical alteration of hydrocarbons in the presence of water: Erdol Kohle-Ergas-Petrochem. Brennstoff-Chemie 26, p. 70–76.

Horsfield, B., Schenk, H.J., Mills, N., and Welte, D.H., 1992, An investigation of the in-reservoir conversion of oil to gas—Compositional and kinetic findings from closed-system programmed-temperature pyrolysis: Advances in Organic Geochemistry, v. 19, p. 191–204.

Jamil, A.S.A., Anwar, M.L., and Kiang, E.S.P., 1991, Geochemistry of selected crude oils from Sabah and Sarawak: Geological Society of Malaysia Bulletin, v. 28, p. 123–149.

Knauss, K.G., Copenhaver, S.A., Braun, R.L., and Burnham, A.K., 1997, Hydrous pyrolysis of New Albany and Phosphoria Shales—Production kinetics of carboxylic acids and light hydrocarbons and interactions between the inorganic and organic chemical systems: Organic Geochemistry, v. 27, p. 477–496.

Pepper, A.S., and Corvi, P.J., 1995, Simple kinetic models of petroleum formation—Part I, Oil and gas generation from kerogen: Marine and Petroleum Geology, v. 12, p. 291–319.

Pepper, A.S., and Dodd, T.A., 1995, Simple kinetic models of petroleum formation—Part II, Oil-gas cracking: Marine and Petroleum Geology, v. 12, p. 321–340.

Price, L.C., 1997, Origins, characteristics, evidence for and economic viabilities of conventional and unconventional gas resource bases,

*in* Dyman, T.S., Rice, D.D., and Westcott, P.A., eds., Geologic controls of deep natural gas resources in the United States: U.S. Geological Survey Bulletin 2146, p. 181–207.

Tsuzuki, N., Yokoyama, Y., Takayama, K., Yokoi, K., Suzuki, M., and Takeda, N., 1997, Kinetic modeling of oil cracking: 1997 Eastern Section American Association of Petroleum Geologists and The Society of Organic Petrology Joint Meeting, Lexington, Kentucky, Abstracts and Program, v. 14, p. 94–96.

Ungerer, P., Espitalié, J., Marquis, F., and Durand, B., 1986, Use of kinetic models of organic matter evolution for the reconstruction of paleotemperatures, *in* Burruss, J., ed., Thermal modeling in sedimentary basins: Paris, Editions Technip., p. 531–546.

Wood, D.A., 1988, Relationships between thermal maturation indices calculated using Arrhenius equation and Lopatin method—Implications for petroleum exploration: American Association of Petroleum Geologists Bulletin, v. 72, p. 115–134.